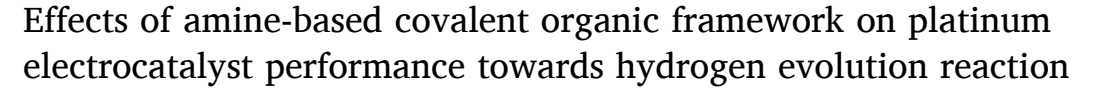
Contents lists available at ScienceDirect

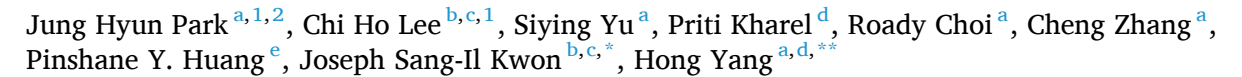
Nano Energy

journal homepage: www.elsevier.com/locate/nanoen



Full paper





- a Department of Chemical and Biomolecular Engineering, University of Illinois at Urbana-Champaign, 600 South Mathews Avenue, Urbana, IL 61801, United States
- ^b Artie McFerrin Department of Chemical Engineering, Texas A&M University, College Station, TX 77843, United States
- Texas A&M Energy Institute, College Station, TX 77843, United States
- ^d Department of Chemistry, University of Illinois at Urbana-Champaign, Urbana, IL 61801, United States
- ^e Department of Materials Science and Engineering, University of Illinois at Urbana-Champaign, Urbana, IL 61801, United States

ARTICLE INFO

Keywords: Covalent organic framework Hydrogen evolution reaction Electrocatalysis HER Solid-liquid interface model

ABSTRACT

Performance of electrocatalyst in an aqueous electrolyte is greatly influenced by the structure of electrolyteelectrocatalyst interface. Regulating mass transfer is important in controlling surface reactions to alter the overall reaction kinetics. Thus, modification of interfacial structures is an effective approach to improving the electrocatalytic performance. In this paper, we report the use of functionalized amine-based covalent organic frameworks (COFs) as the modifier of electrocatalytic properties by facilitating the proton transfer of hydrogen evolution reaction (HER) in an acidic medium. Results from the electrochemical solid-liquid interface (ESLI)based density functional theory (DFT) calculations suggest that functionalized COFs increase the local hydrogen concentration at the COF-electrocatalyst interface. Our simulation data indicates the enhancement in HER activity is achieved partially through the protonation site of the secondary amine of the COF on electrode surface, suggesting a new mode of controlling interfacial proton transfer for improving the HER kinetics.

1. Introduction

Green hydrogen production relies on the development of efficient electrochemical systems [1-3], which require not only active electrocatalysts but also optimal system designs [4]. Since electrocatalysis is often a heterogeneous process occurring in an aqueous electrolyte, its elemental steps involve adsorption of reactant species, reaction of adsorbed species, and desorption of products [5,6]. For example, the performances of electrocatalysts in hydrogen evolution reaction (HER) and oxygen evolution reaction (OER) are heavily influenced by the near-surface chemisorption of reactants (e.g., H2O, OH-, and H+) and reaction intermediates (e.g., H*, HO*, HOO*, and O*) [7]. In this context, modifying interfacial structures may directly affect mass transfer and reaction kinetics, thereby enhance the overall catalytic performance [8–10].

There exist several strategies for modifying interfacial structures and consequently overall electrochemical reaction rates. For instance, enhancing the affinity of reactant ions can be achieved through surface modifications of electrocatalysts, including the Helmholtz plane, using functional molecules [11,12]. One direct result of such modification is high local concentration or accelerated diffusion of reactants. Ionic liquids were used, in this context, to improve the kinetics of oxygen reduction reaction because of their oxygen solubility, which helps increasing oxygen concentration and facilitates rapid removal of water molecules [13,14]. Protic ionic liquid was also utilized to improve the diffusion of protons to catalyst surface [15]. Modification of interfacial structures change interactions between surface atoms and reaction species as well [5]. Such interactions are closely related to the intrinsic properties or local conditions, such as electronic structure of active sites [16], surface strain [17], defects or vacancies [3], and neighboring sites

https://doi.org/10.1016/j.nanoen.2024.109947

Received 29 February 2024; Received in revised form 23 May 2024; Accepted 28 June 2024 Available online 2 July 2024

2211-2855/© 2024 The Authors. Published by Elsevier Ltd. This is an open access article under the CC BY-NC-ND license (http://creativecommons.org/licenses/bync-nd/4.0/).





^{*} Corresponding author at: Artie McFerrin Department of Chemical Engineering, Texas A&M University, College Station, TX 77843, United States.

^{**} Corresponding author at: Department of Chemical and Biomolecular Engineering, University of Illinois at Urbana-Champaign, 600 South Mathews Avenue, Urbana, IL 61801, United States.

E-mail addresses: kwonx075@tamu.edu (J.S.-I. Kwon), hy66@illinois.edu (H. Yang).

 $^{^{\}rm 1}$ These authors contributed equally to this work.

² Current address: Illinois Sustainable Technology Center, University of Illinois at Urbana-Champaign, 1 Hazelwood Drive, Champaign, IL 61820, United States.

Fig. 1. Schematic illustration of distribution of protons at unmodified (left) and COF-modified (right) electrode surfaces.

[18]. While the overall strategy for interfacial modification has been established for a while, the complexity of multistep electrochemical reactions impedes the development of approaches to synergistically increasing the mass transfer and surface reactivity [19], and hinders the identifications of key factors for high catalytic performance [20].

To understand the effect of interfacial structures on proton transfer and reaction kinetics in an electrocatalytic process, such as HER, we designed specific covalent organic frameworks (COFs) for surface modifications of Pt electrocatalysts. The COFs selected in this study possess two-dimensional (2D) structures [21-26]. They were reported to facilitate lithium-ion mitigation in batteries [21,27]. Amine-based 2D COFs exhibit excellent stability across a wide potential window under acidic conditions [28,29]. In addition, these COFs are structurally flexible in terms of modifiable functional groups [30-32]. In this study, we introduced amine (NH2), nitro (NO2) and sulfonic (SO3) functional groups, respectively, to investigate their effects on the interfacial structure and the corresponding electrocatalytic activity. These functional groups may change the electronic properties of amine-based COFs, with NH₂ being an electron donating group, while NO₂ and SO₃ being the electron withdrawing groups. As a result, these functionalized COFs are expected to change the proton distributions in the near-surface region, as illustrated in Fig. 1.

We observed that the NH2-COF-modified Pt electrocatalyst exhibited the greatest enhancement in HER activity, with 30 % lower overpotential at 10 mA cm⁻² than the unmodified Pt. Density functional theory (DFT) simulations were performed based on an electrochemical solid-liquid interface (ESLI) model, which considers all key species on the catalyst surface, including water, proton, COF, and Pt. Our simulation results suggest that incorporating COFs to the systems significantly enhances the proton transfer and consequently the kinetics of hydrogen formation. Protonation on the secondary amine group and electrondonating ability of the functional group (i.e., NH2) help concentrate protons at the interface. Our DFT calculations further suggest that strain of Pt surface increases after its modifications by COFs, favoring a new pathway for the formation of molecular hydrogen, which most likely exists at the researched interface. In this new pathway, two adsorbed hydrogen atoms are not all from Pt surfaces; instead, one from the secondary amine site and the other from the on-top site of Pt surfaces. These two types of absorbed hydrogen atoms have the shortest inter-atom distance and thus facilely react to produce hydrogen molecules.

2. Experimental section

2.1. Chemicals

Mesitylene (98 %), p-dioxane (>99 %), 1,3,5-triformylbenzene (97 %), p-phenylenediamine (>98 %), 2,5-diaminobenzenesulfonic acid (>97 %), ferrocene (>98 %), Nafion solution (5 wt%), and tetrabutylammonium perchlorate (>98 %) were purchased from Sigma

Aldrich. Acetonitrile (>99 %), *N*-methyl-2-pyrrolidone (>99 %), and tin (II) chloride dihydrate (>98 %) were purchased from Alfa Aesar. 2-nitro-*p*-phenylenediamine (95 %), tetrahydrofuran (>99 %), acetone (>99 %), and acetic acid (glacial grade) were obtained from Thermo Fisher Scientific. Triformylphlorogucinol (>95 %) were purchased from AmBeed and Fisher Scientific. Platinum on activated carbon (20 wt%) was provided by BASF. All chemicals were used without further purification.

2.2. Synthesis of Bz-COF and functionalized COFs

In this study, Bz-COF was prepared through Schiff-base reaction. In a typical procedure, triformylphloroglucinol (TPG, 0.15 mmol or 31.5 mg) was mixed with p-phenylenediamine (0.22 mmol or 24.5 mg) in 1.5 mL of a solvent mixture made of mesitylene and 1,4-dioxane (50/50 v/v) in a 5 mL reaction vial. This reaction mixture was heated at 120 °C for 72 h in the presence of 0.3 mL of 0.3 M aqueous acetic acid to produce red powder, which was filtered and washed using 30 mL of water and 30 mL of acetone for three times. The product was dried in a vacuum oven (VWR Symphony) at 80 °C overnight.

For the preparation of NO₂-COF, 34.43 mg of 2-nitro-p-phenylenediamine (instead of p-phenylenediamine) was used, while keeping all other procedures the same. Similarly, 2,5-diaminobenzene sulfonic acid (42.31 mg) was used to make SO₃-COF. NH₂-COF was synthesized by reducing NO₂-COF. In a typical procedure, 50 mg of NO₂-COF and 1.5 g of SnCl₂·2 H₂O were added to a 5 mL of tetrahydrofuran, followed by refluxing for 3 h. The powder product was then washed with 200 mL of 0.1 M HCl aqueous solution.

2.3. Synthesis of Bz-COF2

Bz-COF2 was prepared through Schiff-base reaction between of 1,3,5-triformylbenzene (TFB, 0.15 mmol) and p-phenylenediamine (0.22 mmol) in 1.5 mL of 50:50 (v/v) mesitylene and 1,4-dioxane solvent mixture in a 5 mL reaction vial. The reaction mixture was heated at 120 °C for 72 h in the presence of 0.3 mL of 0.3 M aqueous acetic acid to produce a red powder, which was filtered and washed using 30 mL of water and 30 mL of acetone for three times, respectively. The product was dried under the vacuum at 80 °C overnight.

2.4. Characterization of Bz-COF and functionalized COFs

The chemical structures of the COFs were analyzed after deprotonation of the COFs using 0.1 M KOH aqueous solution to increase its pH value to 8. The FT-IR spectra were recorded using a Perkin Elmer Spectrum 2 FTIR spectrometer equipped with an attenuated total reflection (ATR) module. Solid-state ¹³C NMR spectrum was recorded on a Varian UI300 NMR spectrometer with CP-MAS at a ¹³C frequency of 75.4 MHz under a spinning speed of 10 kHz and the MAS condition with

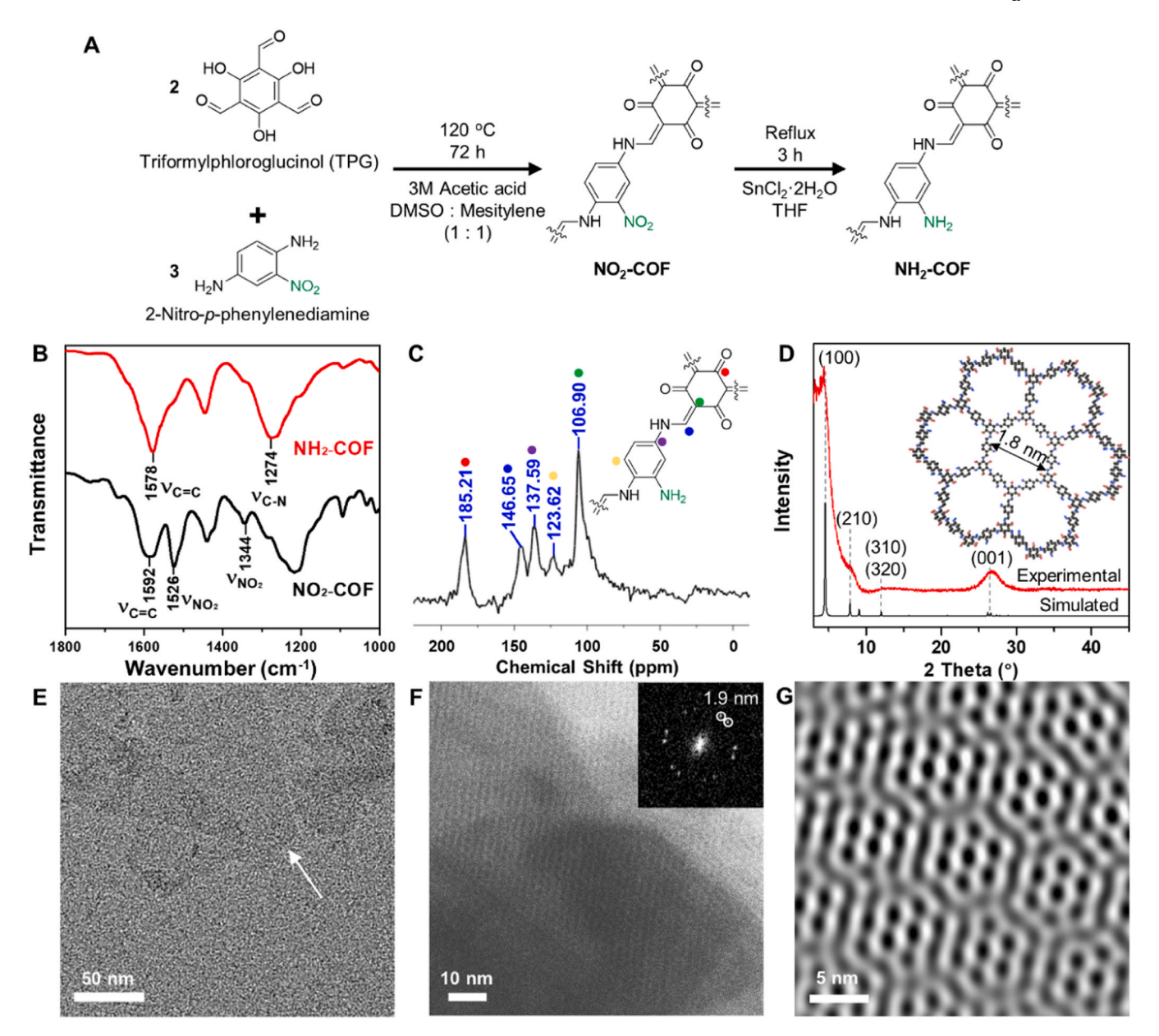


Fig. 2. (a) Synthetic route, (b) FT-IR spectrum, (c) solid-state ¹³C-NMR spectrum, (d) XRD pattern, (e) TEM micrograph, (f) low-dose LAADF STEM image, and (g) Fourier-filtered image of NH₂-COF. Inset in (f) exhibits the corresponding FFT diffractogram. FT-IR spectrum for NO₂-COF is included in (b) for comparison.

3 ms of contact time. Transmission electron microscopy images were obtained using JEOL 2100 Cryo TEM with a LaB₆ emitter at an accelerating voltage of 200 kV. Low-angle annular dark-field scanning transmission electron microscopy was carried out using an aberration corrected Thermo Fisher Themis-Z STEM, operated at 300 kV with a convergence semi-angle of 18 mrad and collection angles of 25–151 mrad. A low electron dose of 100 e $^{\rm c}$ Å $^{\rm -2}$ was used to record the pores to minimize radiation damage. TEM samples were prepared by drop casting a sample suspension onto holey carbon-coated TEM grid. Powder XRD patterns were recorded on Rigaku Miniflex 600 diffractometer using Cu K α radiation ($\lambda=1.5418$ Å). Elemental analysis of C, H, and N were conducted using Exeter Analytical CE-440 Elemental Analyzer.

2.5. Preparation of COF-modified Pt electrocatalysts

In a typical procedure, the amount of COF was calculated based on the molecular weight of the repeating unit of each COF (see Table S1). Four micromoles of a COF (i.e., 2.5 mg of Bz-COF, 3.1 mg of NO₂-COF,

2.7 mg of NH2-COF, and 3.5 mg of SO3-COF) was mixed with 2 mL of NMP in 2 mL vial and sonicated for 120 min in a sonicator bath (Branson CPX2800H) to make a stock solution/suspension at a concentration of 2 μmol/mL. Similarly, 32 mg of carbon-supported Pt was added to 4 mL of NMP and sonicated for 60 min to make the stock suspension at a concentration of 8 mg/mL. To make a 0.1 µmol COF-modified Pt catalyst, $50\,\mu L$ of the COF dispersion in NMP was added to $0.25\,mL$ of Pt dispersion in microtube. An additional NMP was added up to 1 mL and the mixture was sonicated for 30 min in bath sonicator. The resulting suspension was centrifuged at 12,000 rpm for 5 min to remove NMP, followed by drying under vacuum at 80 °C for 6 h and cooling down to room temperature at ambient atmosphere to get the COF-modified Pt electrocatalyst. The same general procedure was used to make the COFmodified Pt electrocatalyst, except the amount of COF was 0.2 µmol (100 μ L of the stock solution/suspension), 1 μ mol (500 μ L), and 2 μ mol (1000 μ L), in 0.25 mL of Pt dispersion.

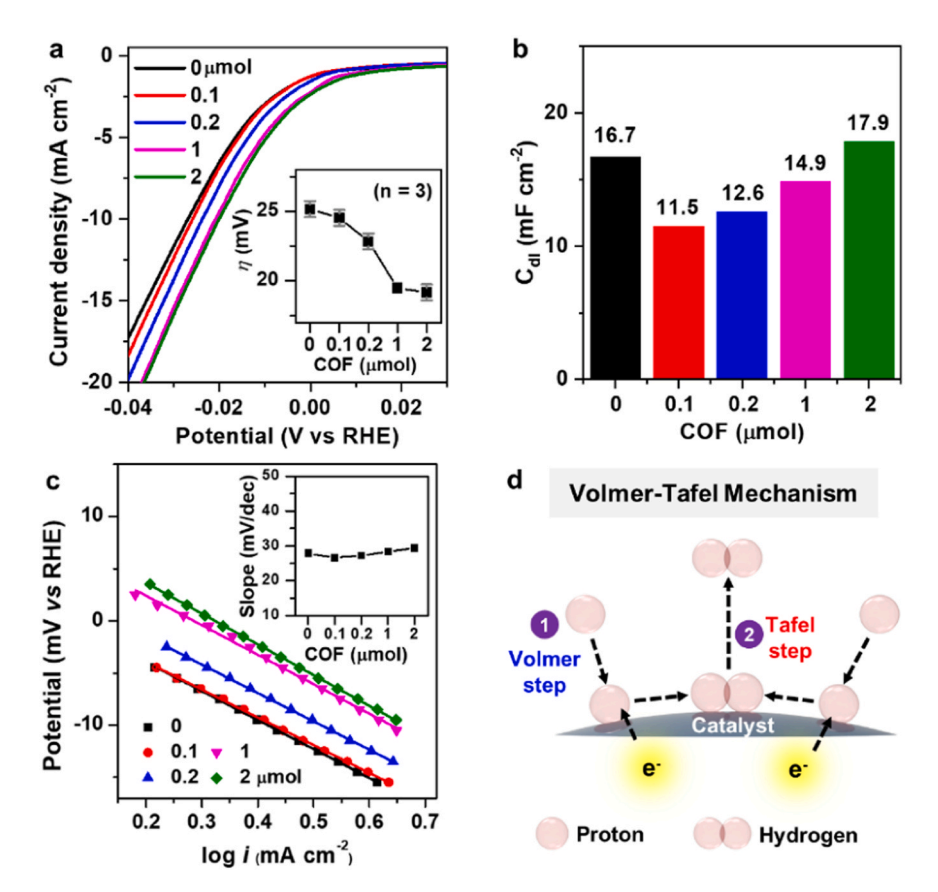


Fig. 3. (a) Polarization curves, (b) double-layer capacitance, (c) Tafel plot of HER activity catalyzed by NH_2 -COF-modified Pt, and (d) illustration of the Volmer-Tafel mechanism. Inset in (a) shows the overpotential at 10 mA cm⁻² and in (c) exhibits the Tafel slopes as a function of the amount of NH_2 -COF.

2.6. Measurements of electrochemical activity

All electrochemical measurements were performed using a potentiostat equipped with a typical three-electrode system, including a glassy carbon rotating disk electrode (RDE, 5 mm diameter) as the working electrode, a Pt wire as the counter, and a reversible hydrogen electrode (RHE, Hydroflex) as the reference in a N_2 -saturated 0.5 M $H_2 SO_4$ solution at room temperature. The potential of reference electrode was calibrated based on hydrogen evolution and oxidation reaction. The catalyst ink was prepared by adding 485 μL of ethanol and 15 μL of Nafion solution to COF-modified Pt, followed by sonication for 5 min. Ten microliter of the catalyst ink was dropped on a RDE to prepare the working electrode with a mass loading of 0.2 mg cm $^{-2}$. Control experiments in the alkaline electrolytes were carried out following the same procedures except the solution was changed to 0.1 M KOH.

Linear sweep voltammetry (LSV) was conducted at a scan rate of $10~\text{mV}~\text{s}^{-1}$ using the RDE working electrode without rotation. Three independent runs were typically carried out to obtain a data point, such as overpotential, at a given condition. Double-layer capacitance (C_{dl}) was determined by cyclic voltammetry (CV). The CV measurement was carried out with a scan rate ranging from 5 to 25 mV s⁻¹ in the non-Faradaic region from 0.04 to 0.14 V (vs. RHE). The change in current density ($\Delta J = J_a J_c$) at 88 mV was plotted as a function of scan rate, and the C_{dl} value was obtained from the slope after being divided by two.

The potential window of COFs was measured using a potentiostat equipped with a standard three-electrode system, including a RDE (5 mm diameter) as the working electrode, a Pt wire as the counter, and a silver wire as the quasi-reference electrode in a $N_2\text{-saturated}$ acetonitrile at room temperature. Tetrabutylammonium perchlorate (0.2 M) was used as the electrolyte. The potential of reference electrode was calibrated using ferrocene and the CV measurement was carried out in the potential region from -1.1 to 1.9 V (vs. SCE).

2.7. Quantum mechanics simulations

All ab initio calculations were performed with the Vienna Ab initio Simulation Package (VASP 5.4.4) [33]. The Perdew-Burke-Ernzerhof (PBE) [34] exchange-correlation functions and the projector augmented wave (PAW) method [35] with a generalized gradient approximation (GGA) [34] were used to obtain the chemisorption energy on the surface. The Monkhorst-Pack [36] k-point grid was used, and maximum symmetry was applied to reduce the number of k-points in all calculations. A plane-wave cut-off energy was set at 500 eV. Lattice constants and internal atomic positions were optimized until the residual forces became less than 0.02 eV/Å. The spin polarization and dipole correction were also included to decouple the electrostatic interaction between repeated surface structures. Valence orbital of active sites was obtained by the partial density of state (PDOS), which was calculated by sampling the Brillouin zone with a 10 \times 10 x 1 k-point grid. Four different COF structures (Bz-COF, NO2-COF, NH2-COF, and SO3-COF) and Pt (111) surface were modelled in this study. The Pt (111) surface was constructed using four atomic layers and atoms in the bottom two layers were fixed while those in the top two layers were allowed to fully relax. The vacuum slab space of a unit cell in the z-direction was set to 15 Å to avoid interactions between layers. To investigate HER kinetics for designed surfaces, we used the electrochemical solid-liquid interface (ESLI) model [37], which includes catalytic surface, adsorbent, and water layer. The activation energy barriers were calculated using the climbing image nudged elastic band (CI-NEB) method by considering five images between the initial and final states [38].

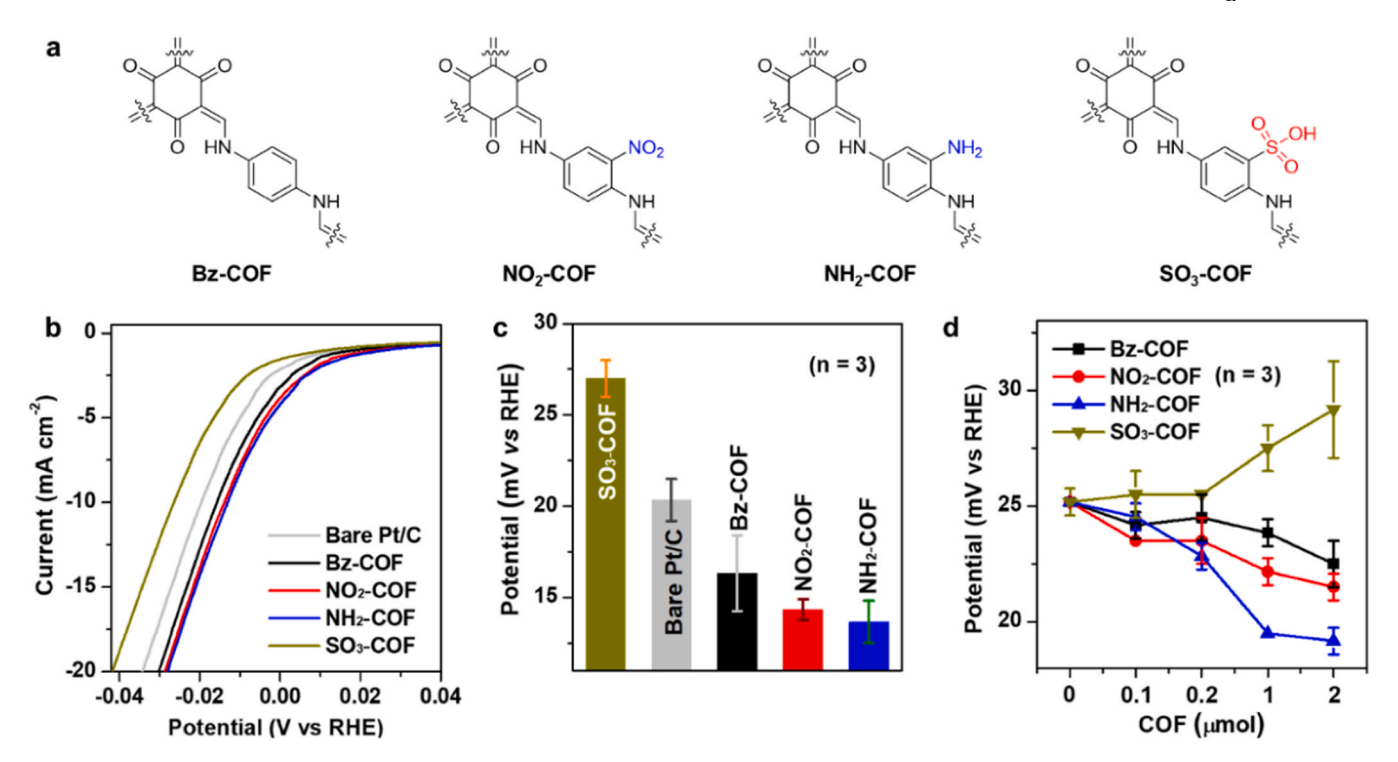


Fig. 4. Pt electrocatalysts with (a) functionalized COFs, and their (b) polarization curves, and HER performances characterized by overpotentials at (c) 10 mA cm^{-2} (COFs: $2 \text{ }\mu\text{mol}$) and (d) as a function of the COF amount used.

3. Results and discussion

3.1. Preparation and characterization of functionalized COFs

The NO2-COF was synthesized via the Schiff-base reaction using triformylphloroglucinol (TPG) and 2-nitro-p-phenylenediamine as the precursors and acetic acid as the catalyst (Fig. 2a and Fig. S1). The Fourier-transform infrared (FT-IR) spectra exhibit the stretching mode of the bridging C=C bond at 1592 cm^{-1} , and the stretching modes of the NO_2 moiety at 1526 and 1344 cm^{-1} (Fig. 2b) [29]. Noticeably, the stretching mode of the C=O of TPG at 1642 cm⁻¹ is absent in the spectrum (Fig. S2), indicating the successful synthesis of NO₂-COF from TPG. The as-made NO2-COF was subsequently reduced to NH2-COF using SnCl2 as the reducing agent. In the NH2-COF spectrum, the two characteristic IR peaks of the nitro group disappeared, while the peak for the C=C stretching mode moved from 1592 to 1578 cm⁻¹ with additional peak appearing at 1274 cm⁻¹, which can be assigned to C-N_{amine} (Fig. 2b). This shift is a consequence of the change in electronegativity and its resonance effect on the COF structure, which resulted from the reduction of the nitro group [39]. The elemental composition analysis reveals that the H/N mass ratio increased from 0.20 (NO2-COF) to 0.23 (NH₂-COF), which agrees with the results obtained from the calculation (Table S2), thus further confirming the successful reduction. A solid-state ¹³C nuclear magnetic resonance (NMR) study indicates that the reduction product contains C=O (185.21 ppm), C=C-N (146.65 ppm), C_2 -C-N (137.59 ppm), C- C_2 (123.62 ppm), and C- C_3 (106.90 ppm), indicating the formation of NH2-COF through tautomerization (Fig. 2c) [29].

Fig. 2d shows the powder X-ray diffraction (XRD) pattern of the NH₂-COF, and the simulated pattern derived from the density functional tight binding (DFTB) method [29]. The characteristic (100) diffraction for this COF structure was observed at 4.24° 2 θ , in good agreement with the simulation results (4.5° 2 θ). The shoulder peak at 7.6° 2 θ is attributed to (210) plane of NH₂-COF, and the peak at 26.6° 2 θ could be assigned to (001) diffraction [40]. The XRD data reveals that NH₂-COF has a hexagonal symmetry with a wall-to-wall distance of 1.8 nm and an

interlayer space of 0.32 nm, as illustrated in Fig. 2d. The XRD results further indicate that the NH2-COF is less ordered than NO2-COF, as suggested by the weaker diffraction intensity and fewer defined peaks in Fig. S3 [41]. Transmission electron microscopy (TEM) studies reveal that the NH₂-COF possesses a sheet-like morphology (Fig. 2e). High-magnification image (Fig. 2f) obtained using low-angle annular dark-field scanning TEM (LAADF-STEM) visualizes the porous structure of NH2-COF. The image and the corresponding fast Fourier transform (FFT) diffractogram (Fig. 2f inset) show that the NH2-COF is crystalline with a lattice spacing of ~ 1.9 nm, which agrees with the XRD analysis and N₂ isotherm analysis (Fig. 2d and Fig. S4). In this specific region, the COF layers are twisted relative to one another at 16° angle, resulting in a Moiré pattern that is clearly visible in the Fourier-filtered image (Fig. 2g). Such sheet-like morphology favored the van der Waals interaction between the COFs and substrate, which enables a close contact between the NH₂-COF layer and Pt surface [42].

3.2. Study of the HER performance of COF-modified Pt electrocatalysts

The functionalized COFs were dispersed in N-methyl-2-pyrrolidone (NMP) and mixed with a Pt catalyst to prepare a COF-modified Pt electrocatalyst on carbon support. The electrochemical stability of NH2-COF was tested in N2-saturated acetonitrile, using a potential range from -1.1 to 1.9 V (vs. SCE). Notably, we detected no significant redox peaks within the potential window from -0.8 to 1.7 V (vs. SCE), indicating remarkable electrochemical stability (Fig. S5). The polarization curves of the NH2-COF modified Pt exhibited enhanced HER activity in comparison with the pristine Pt (Fig. 3a). Control experiments using NH₂-COF alone barely revealed any HER activity from -0.04 to 0.0 V (vs. RHE) (Fig. S6). Based on these findings, we attributed the enhanced HER activity to the interaction between NH2-COF and Pt. We evaluated the overpotential (η) at 10 mA cm⁻² using different quantities of NH₂-COF (inset in Fig. 3a). The NH2-COF modified Pt exhibited an overpotential of 19 mV at a COF loading of 2 µmol. This corresponds to an overpotential reduction of approximately 30 % in comparison to the pristine Pt electrocatalyst (26.7 mV). At the same overpotential, the HER current

density increased with the higher amount of NH2-COF.

Capacitances of Pt and COF-modified Pt electrocatalysts were characterized by measuring the electric double layers (EDLs). This EDL is sensitive to the electronic structure at the interface [43,44]. Our results show the double-layer capacitance (C_{dl}) changed from 16.7 mF cm $^{-2}$ for Pt to 11.5 mF cm $^{-2}$ for 0.1 µmol NH₂-COF-modified Pt (Fig. 3b, Fig. S7-S8). The control experiment using only NH₂-COF exhibited a negligible C_{dl} value of 0.00015 mF cm $^{-2}$ (Fig. S9). These results suggest that the observed changes in C_{dl} result from the interaction between NH₂-COF and Pt surface. As the amount of NH₂-COF changed from 0.1 to 2 µmol, C_{dl} rose from 11.5 to 17.9 mF cm $^{-2}$. The data suggests adding NH₂-COF greatly change the thickness of the electric double layer or charge density at the interface region.

We investigated the HER mechanisms of these COF-modified Pt electrocatalysts by firstly examining the Tafel plots [45]. The NH₂-COF-modified Pt exhibited a Tafel slope of about 30 mV/dec, which changed little when other amounts were used to modify the Pt catalyst (Fig. 3c). Such a small Tafel slope is an indicator of Volmer-Tafel mechanism (Fig. 3d). In this mechanism, the rate-limiting step (RLS) is the Tafel step, during which two adsorbed hydrogens combine to generate one hydrogen molecule, though the nature of adsorbed hydrogens could be quite different between COF-modified and pristine Pt catalysts, which we will discuss in the following sections. Notably, the surface modification of Pt catalyst with NH2-COF resulted in a decrease in the overall resistance of charge transfer in HER (Fig. S10). In addition, the NH2-COF enhanced the electrochemical stability of the modified Pt/C catalyst, as illustrated in the chronoamperometric test (Fig. S11). No aggregation of Pt nanoparticles was observed after the stability test (Fig. S12). The slight change in C_{dl} from 17.9 to 17.6 mF cm⁻² after the stability test also implied negligible variation of COF layer on Pt/C catalyst (Fig. S13).

3.3. Study of the influence of COF modifications on HER activity

COFs with a functional group other than amine (-NH₂) were synthesized to study the impact of functionalization on HER activity. In addition, the amine-COF without any functional group (Bz-COF) and one with sulfonate group (SO₃-COF) were made to examine how electronic structures of COFs affect proton transfer and catalytic performance. Bz-COF and SO₃-COF were synthesized by substituting 2-nitro-p-phenylenediamine with p-phenylenediamine and 2,5-diaminobenzenesulfonic acid, respectively, and their structures were characterized using FT-IR spectroscopy, solid-state 13 C NMR, and powder XRD (Fig. S1 and S14-S16).

Fig. 4a shows chemical structures of Bz-COF, NO₂-COF, NH₂-COF, and SO₃-COF. Their HER activity was evaluated by analyzing the polarization curves of Pt electrocatalysts modified by 2 μ mol of Bz-COF, NO₂-COF, NH₂-COF, and SO₃-COF, respectively (Fig. 4b). The results reveal the following trend in HER activity: SO₃-COF < pristine Pt (no-COF) < Bz-COF < NO₂-COF < NH₂-COF. The SO₃-COF modified Pt exhibits an overpotential of 29.2 mV at the current density of 10 mA cm $^{-2}$, which is higher than that of bare Pt/C electrocatalyst (26.7 mV). In contrast, Bz-COF, NO₂-COF, and NH₂-COF modified Pt exhibited overpotentials of 22.5, 21.5, and 19.2 mV, respectively (Fig. 4c). The enhanced HER performance of Bz-COF modified Pt suggests the HER activity is synergistically affected by both the functional group (-NO₂, -NH₂, -SO₃) and the secondary amine site in the basic COF structure.

To understand the structural origin for the observed HER performance, we examined the effects of different functional groups. Sulfonate group is known to have good proton conductivity [46–48], and SO₃-COF modified electrode was expected to enhance HER activity by facilitating proton transfer to Pt surface. Our experimental observations however show that as the loading amount of SO₃-COF increased, the observed overpotential grew, indicating the HER activity deteriorated (Fig. 4d). The detrimental effect may rise from the poisoning of active sites because of the high affinity of sulfonate group to Pt [49,50]. This

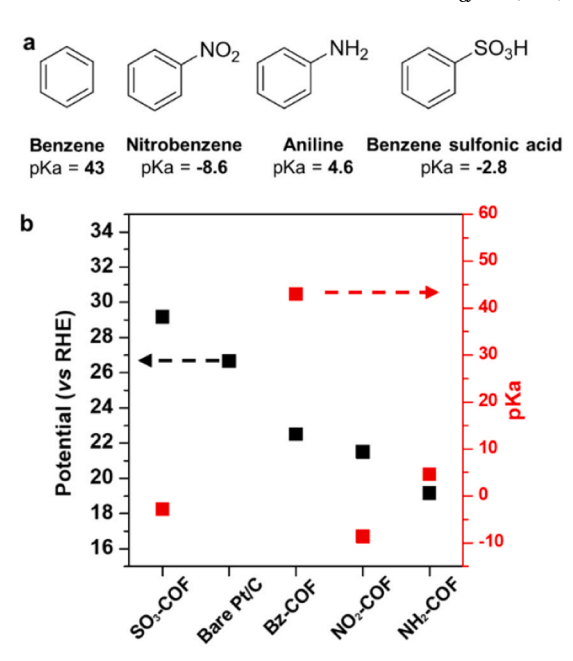


Fig. 5.. (a) Estimated pK_a values for different COFs, and (b) relationship between overpotential and estimated pK_a value of the corresponding functional group.

argument is supported by the observation of enhanced HER performance for those catalysts with nitro and amine functional groups, which did not poison the Pt surface. The change in activity has been attributed to interfacial proton transfer within the tightly bonded Helmholtz layer or Stern layers [51,52]. NH2-COF modified electrode did not exhibit catalytic activity enhancement for HER in a 0.1 M KOH solution. This observation is readily understood because of the scarcity of protons in alkaline electrolytes and the HER typically does not undergo proton transfer pathway in alkaline media (Fig. S17). To investigate whether the functional groups of COFs are directly involved in the protonation process, we analyzed the relationship between pKa values of functionalized COFs and HER activity catalyzed by these COF-modified Pt/C (Fig. 5a). The estimated pK_a value for the aniline moiety of NH₂-COF is approximately 4.6, suggesting that it could be protonated under acidic conditions. Therefore, NH2-COF may provide a pathway for proton transfer to NH2-COF-Pt interface. According to the conventional Volmer-Tafel mechanism, overpotential should have a linear relationship with the pKa of the COFs. Since there exists no clear correlation between pK_a value and overpotential (Fig. 5b), these functional groups may not directly involve in the protonation process.

Despite the different effects of functionalized COFs on HER activity, it is noteworthy to point out that all modified Pt electrocatalysts exhibited similar Tafel slopes (<30 mV/dec), which follow the Volmer-Tafel mechanism (Fig. S18). Thus, we further examined the role of the bridging secondary amine using a COF without the functional groups (Bz-COF2). Bz-COF2 is also stable within the potential window used in this study and thus suited for conducting HER measurements (Fig. S19). Bz-COF2 was synthesized by reacting p-phenylenediamine with 1,3,5triformylbenzene (TFB), which does not have the ketone group (Fig. S20). Bz-COF2 was characterized by FT-IR spectroscopy, solid-state 13 C-NMR spectroscopy, and powder XRD. The peak at 1692 cm $^{-1}$ in FT-IR, which is attributed to the stretching vibration mode of C=O in TFB, disappeared after the reaction (Fig. S21). Solid-state ¹³C-NMR spectrum shows the product exhibits chemical shifts at 157.99 ppm for C-C=N, 149.10 ppm for C₂-C-N, 137.07 ppm for C-C₃, and 130.86 ppm and 121.96 ppm, respectively, for the two C-C2, (Fig. S22). The absence of the peak centered around 184–186 ppm indicates the disappearance of C=O after the reaction, which is consistent with results from the FT-IR spectrum. These convergent results indicate the successful formation of

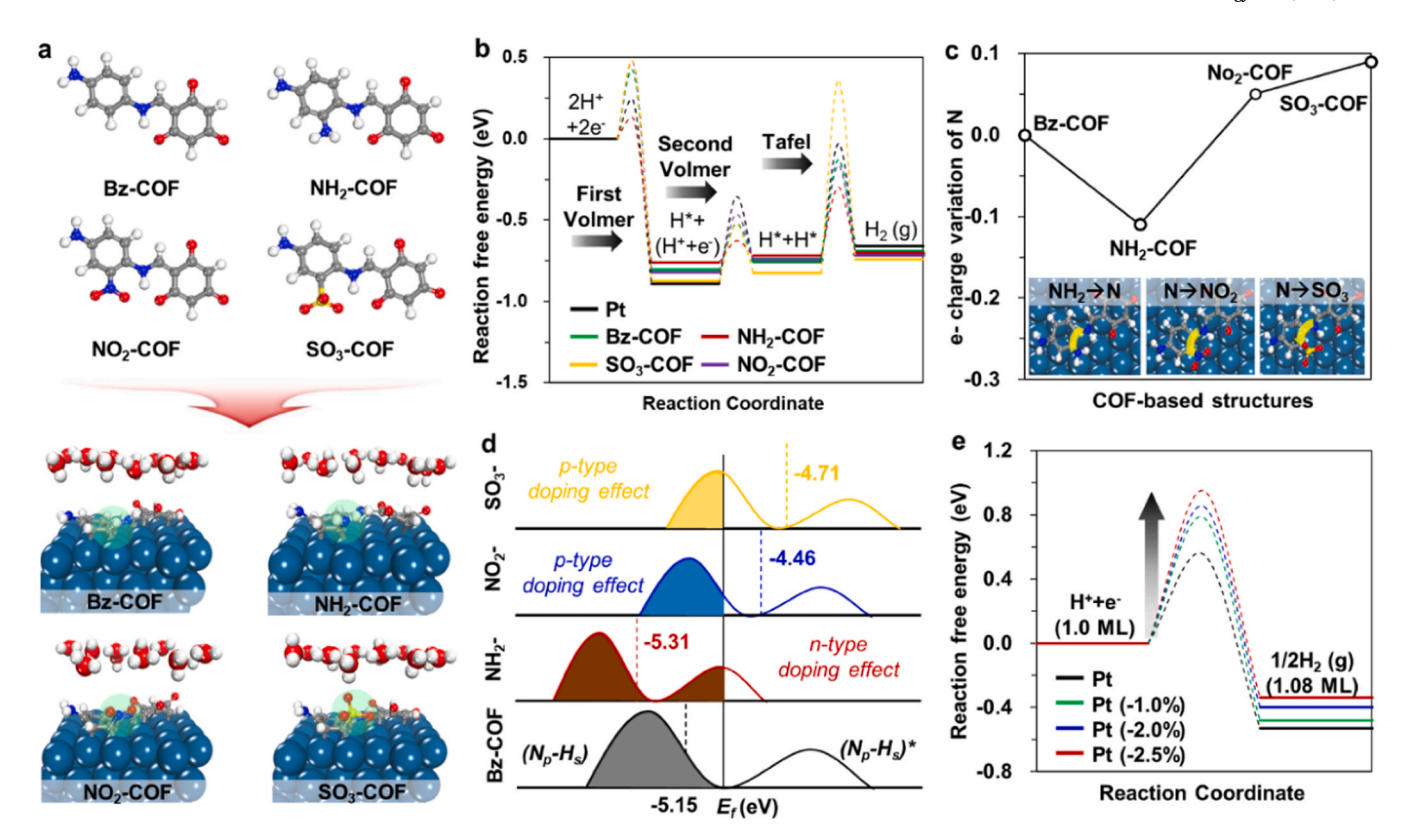


Fig. 6. ESLI-based DFT simulations of COF-modified Pt electrocatalysts. (a) Structures of COF moieties with different functional groups (Bz-COF, NH₂-COF, NO₂-COF, and SO₃-COF) and the illustration of interfacial structures of Pt (111) surface with COF and water layer; (b) overall HER free energy diagram (FED); (c) variation of electron charge of the secondary amine in the framework as a function of different moieties (NH₂, NO₂, and SO₃); (d) p-band centers of secondary amine in the COF-based structures; and (e) FED for HER catalyzed by Pt with a compressive strain of 0, -1, -2, and -2.5 %, respectively.

the Schiff-base compound. Powder XRD pattern shows the formation of ordered framework structures (Fig. S23).

Linear sweep voltammograms reveal that Bz-COF2-modified Pt catalyst exhibits a lowered overpotential, and better activity than pristine Pt toward HER (Fig. S24). This result indicates lacking ketone group and other functional groups in Bz-COF2 does not significantly impact the HER activity. This finding, together with observations from the NH₂-COF-Pt electrocatalyst, suggests that nitrogen-containing bridging structures (C-NH-C and C—N-C) of COFs are important factors for the enhanced HER activity.

3.4. DFT calculation for understanding the effects of functionalized COFs on HER activity

To understand how electrolyte-electrocatalyst interfacial interactions facilitate the transfer of protons, we conducted DFT calculations using the electrochemical solid-liquid interface (ESLI) model (Fig. 6a) [37]. We used the ESLI model so that all major interfacial species could be accounted for in computing the reaction kinetics for proton-electron transfer reactions. In another word, we considered not only Pt surface but also the synergistic effects of solvent (i.e., water), functionalized COF, and acidic environment (Fig. S25) [53]. Specifically, we evaluated the reaction kinetics by comparing activation energy barriers of the elementary steps across the free energy diagram (FED) due to addition of COF. All energy barriers were calculated in the presence of water with proton that is transferred to the adsorbed sites. This design of FED was based on and supported by the experimental results from Tafel slope analysis (Fig. S18). The FED results suggest that the proton combination acts as the rate-limiting step (RLS) judging by the activation energy, which ranges from 0 to 1.2 eV (Fig. 6b). This value is significantly higher than the energy barriers of the Volmer step, which spans from 0 to 0.6 eV for all Pt electrocatalysts, with or without the modification by COFs. Fig. S26 summarizes the calculated energy barriers of the Volmer step for all electrocatalysts, which suggest the Pt electrocatalyst modified by NH₂-COF has the lowest activation energy. In the subsequent Tafel step, where surface protons are taken into the consideration, the ESLI model further indicates the activation energy of NH₂-COF-modified Pt remains the lowest (Fig. S27).

To computationally examine the origin of the change in activation energy of COF-modified Pt surfaces, we first analyzed the binding energy of H* on the Pt(111) facet by considering the geometric effect of active sites, including face-centered cubic (fcc), hexagonally close-packed (hcp), on-top, and bridge sites (Fig. S28). Our calculations indicate that the first tightly bonded layer on Pt(111) surface consists of H* atoms occupying on-top sites, and additional H* atoms on hollow sites (i.e., hcp and fcc), resulting in an optimal surface of 1.08 monolayer (mL) of H* on pristine Pt. Adding COFs may increase proton concentration on the Pt surface. Among the functionalized COFs, NH₂-COF exhibits the highest surface coverage, up to 1.16 mL of H* (Fig. S29), which is consistent with our experimental data based on the capacitance measurements. The enhanced surface proton concentration could contribute to the lowered HER overpotential observed in NH₂-COF modified Pt electrocatalyst.

Our experimental data also suggests the bridging secondary amine site (C-NH-C and C=N-C) is likely the protonation site for proton to transfer from electrolyte to Pt surface. In addition to the adsorbed H* on Pt (i.e., the classical Volmer-Tafel mechanism), the proton at the secondary amine site of COFs needs to be considered in examining both protonation and the subsequent deprotonation step for the formation of hydrogen molecule. We studied the changes in electron charge at the secondary amine of COFs with and without the functional groups of NH₂, NO₂, and SO₃ (Fig. 6c). The modification with COFs leads to the difference in electron-filling in the antibonding states. NH₂ functional group donates electrons to the secondary amine, while the NO₂ and SO₃

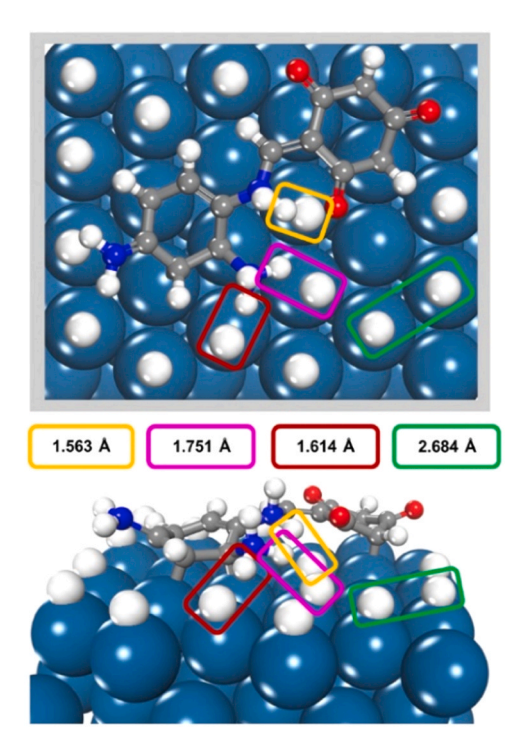


Fig. 7. Illustrations of DFT simulation results of the distance between different types of surface H atoms at water-COF-Pt interface of the electrocatalyst modified with NH₂-COF.

groups extract electrons. Thus, the secondary amine of $\mathrm{NH}_2\text{-}\mathrm{COF}$ exists within a reductive environment, in which protonation at this site becomes easier than that of other COFs.

To further examine the effect of deprotonation of H^* during the surface reaction, we calculated band centers of secondary amines to understand the distribution of valence p-orbitals, which are closely related to the hydrogen binding strength (Fig. 6d). In these functionalized COFs, p-band center shifts either downwards due to an n-type doping effect (i.e., electron donation from NH₂) or upwards due to a p-type doping effect (i.e., electron withdrawal to NO₂ and SO₃). The amine site of NH₂-COF exhibits the lowest p-band center among all the functionalized COFs. This configuration results in more electron filling in the antibonding orbitals, especially those between the p-orbital of nitrogen and s-orbital of hydrogen. As a result, the deprotonation of H^* is favored.

In addition to the deprotonated H* originating from functionalized COFs, additional hydrogen is needed to form molecular hydrogen. Our experimental findings suggest the ability of incorporated COFs to interact with both these hydrogens enhances the efficiency of the formation of molecular hydrogen. Thus, additional DFT simulations were carried out to reveal that COF modification may lead to a reduction in the Pt-Pt distance, changing from 2.775 Å to 2.703 Å (Fig. S30), where

the surface may exhibit a compressive strain up to -2.5 %. The compressive strain, as is suggested by DFT results, is big enough to change the surface reaction kinetics. We therefore performed the DFT calculation to obtain the free energy values for surface reactions on Pt with one monolayer of surface-bound H* atoms and a water bilayer. Specifically, the H* binding free energy on the hollow site was compared among these electrocatalysts according to the magnitude of compressive strain, knowing the optimal H* coverage on Pt is 1.08 mL. All simulations were conducted by considering the water layer on the catalyst surface. The results suggest that as the compressive strain of Pt surface increases, the reaction rate of additional H* binding to the hollow site becomes slow (Fig. 6e). This change can be attributed to the reduced distance between H* on adjacent on-top sites due to the surface stress. The reduced Pt-Pt distance results in electrostatic repulsion and in destabilizing the addition of H* to hollow sites. Consequently, on-top sites become the most favorable position on Pt surface for reactive H* atoms. Crucially, among all hydrogen atoms at the interface of COFmodified Pt, the one stabilized by the secondary amine of COFs becomes the closest to the reactive H* on the on-top site on Pt (1.563 Å), making these two the most likely sources to form a hydrogen molecule (Fig. 7). In another word, hydrogen stabilized by the bridging amine site of COF and H* on the on-top site of Pt react to form one hydrogen molecule, instead of the commonly known situation where two H* atoms on Pt surface react (Fig. 8).

This surface or interface reaction model could explain the observed experimental results, in which Pt modified by NO₂-COF exhibited significantly higher activity than that by SO₃-COF, despite their similarities in both the total number of surface hydrogen atoms and the Pt-Pt distance. In this interfacial reaction pathway, H atom on the amine site is located close to the NO₂ functional group, where protons are stabilized through the electrostatic interaction with oxygen (-0.42 e $\dot{}$) (Fig. S31). Proton interacts however much stronger with oxygen in SO₃-COF (-1.24 e $\dot{}$) than that in NO₂-COF, resulting in a considerable increase in the energy barrier through trapping two protons in transition state (Fig. S27). Our DFT calculations suggest that incorporation of COFs plays a significant role in both increase in surface proton concentration and enhancement in surface reaction kinetics.

4. Conclusion

We showed functionalized amine-based COFs could serve as an effective modifier for Pt electrocatalysts. Quantum simulation results suggest these COFs facilitate the proton transfer and hydrogen molecule formation through the secondary amine of the surface COF. Unlike the pure metal electrode, the formation of hydrogen molecules by COF-modified Pt electrocatalyst may take place between one hydrogen atom from the secondary amine site and another from Pt surface. Such combination to form a hydrogen molecule is an energetically favored pathway for HER under the researched conditions. This study highlights the potential for using functionalized COFs in controlling the interfacial structures of electrocatalysts for high catalytic performance. We

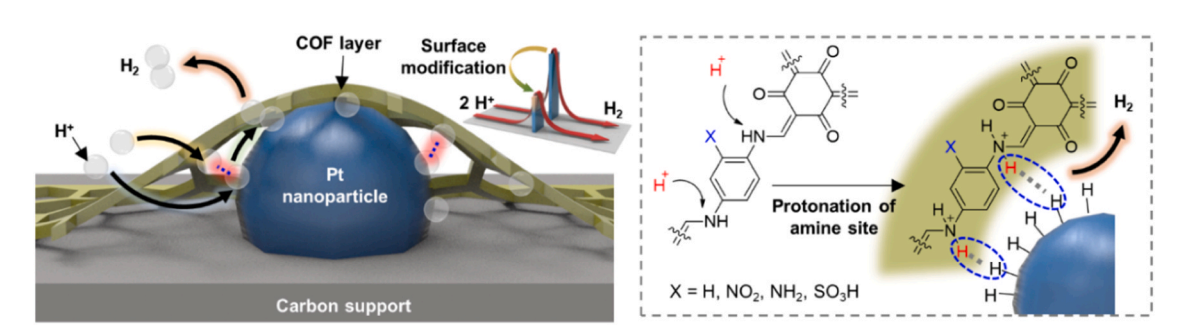


Fig. 8. Schematic illustration of interfacial structures and functions of amine-based COF on HER. Results from DFT simulation suggest the secondary amine in the surface COF framework involves in the formation of hydrogen molecules.

envision this study should provide useful insights into the design of new electrocatalysts using highly ordered porous, thin-film materials, such as functionalized COFs presented in this study.

CRediT authorship contribution statement

Jung Hyun Park: Writing – review & editing, Writing – original draft, Validation, Methodology, Investigation, Formal analysis, Data curation, Conceptualization. Chi Ho Lee: Writing – review & editing, Writing – original draft, Validation, Methodology, Investigation, Formal analysis, Data curation, Conceptualization. Siying Yu: Writing – review & editing, Writing – original draft, Data curation. Priti Kharel: Data curation. Roady Choi: Data curation. Cheng Zhang: Data curation. Pinshane Y. Huang: Resources, Investigation. Joseph Sang-Il Kwon: Writing – review & editing, Supervision, Resources, Investigation, Funding acquisition, Conceptualization. Hong Yang: Writing – review & editing, Supervision, Funding acquisition, Conceptualization.

Declaration of Competing Interest

The authors declare that they have no known competing financial interests or personal relationships that could have appeared to influence the work reported in this paper.

Data availability

Data will be made available on request.

Acknowledgments

This research was supported by National Science Foundation (NSF-2055734), Packard Foundation Fellowship program, Basic Science Research Program through National Research Foundation of Korea (NRF, 2021R1A6A3A03040418), University of Illinois, and Artie McFerrin Department of Chemical Engineering and Energy Institute of Texas A&M University. Powder X-ray diffraction was performed in George L. Clark X-Ray Facility and 3 M Materials Laboratory in School of Chemical Sciences (SCS) at the University of Illinois, Urbana-Champaign (UIUC). The NMR study was carried out in the NMR laboratory in SCS at UIUC. Elemental analysis was conducted in the Microanalysis Laboratory in SCS at UIUC. Electron microscopy was carried out in Materials Research Laboratory Central Facilities at UIUC.

Appendix A. Supporting information

Supplementary data associated with this article can be found in the online version at doi:10.1016/j.nanoen.2024.109947.

References

- [1] S. Chu, Y. Cui, N. Liu, The path towards sustainable energy, Nat. Mater. 16 (2017) 16-22, https://doi.org/10.1038/nmat4834.
- [2] N. Dubouis, A. Grimaud, The hydrogen evolution reaction: from material to interfacial descriptors, Chem. Sci. 10 (2019) 9165–9181, https://doi.org/10.1039/ C9SC03831K.
- [3] H. Tan, et al., Engineering a local acid-like environment in alkaline medium for efficient hydrogen evolution reaction, Nat. Commun. 13 (2022) 2024, https://doi. org/10.1038/s41467-022-29710-w.
- [4] J. Guo, et al., Direct seawater electrolysis by adjusting the local reaction environment of a catalyst, Nat. Energy 8 (2023) 264–272, https://doi.org/ 10.1038/s41560-023-01195-x.
- [5] A. Kulkarni, S. Siahrostami, A. Patel, J.K. Nørskov, Understanding catalytic activity trends in the oxygen reduction reaction, Chem. Rev. 118 (2018) 2302–2312, https://doi.org/10.1021/acs.chemrev.7b00488.
- [6] J.S. Yoo, X. Rong, Y. Liu, A.M. Kolpak, Role of lattice oxygen participation in understanding trends in the oxygen evolution reaction on perovskites, ACS Catal. 8 (2018) 4628–4636, https://doi.org/10.1021/acscatal.8b00612.

- [7] Y. Qiu, et al., Proton relay for the rate enhancement of electrochemical hydrogen reactions at heterogeneous interfaces, J. Am. Chem. Soc. 145 (2023) 26016–26027, https://doi.org/10.1021/jacs.3c06398.
- [8] K. Zhao, et al., Enhancing hydrogen oxidation and evolution kinetics by tuning the interfacial hydrogen-bonding environment on functionalized platinum surfaces, Angew. Chem. Int. Ed. 61 (2022) e202207197, https://doi.org/10.1002/ pairs 202207107
- [9] L. Zou, et al., Lattice doping regulated interfacial reactions in cathode for enhanced cycling stability, Nat. Commun. 10 (2019) 3447, https://doi.org/10.1038/s41467-019-11299-2.
- [10] Y. Li, et al., Interfacial engineering of polycrystalline Pt₅P₂ nanocrystals and amorphous nickel phosphate nanorods for electrocatalytic alkaline hydrogen evolution, Small 19 (2023) 2206859, https://doi.org/10.1002/smll.202206859.
- [11] S. Yu, et al., Nanoparticle assembly induced ligand interactions for enhanced electrocatalytic CO₂ conversion, J. Am. Chem. Soc. 143 (2021) 19919–19927, https://doi.org/10.1021/jacs.1c09777.
- [12] X. Chen, et al., Electrochemical CO₂-to-ethylene conversion on polyamine-incorporated Cu electrodes, Nat. Catal. 4 (2021) 20–27, https://doi.org/10.1038/s41929-020-00547-0.
- [13] S. Favero, I.E.L. Stephens, M.M. Titirici, Engineering the electrochemical interface of oxygen reduction electrocatalysts with ionic liquids: a review, Adv. Energy Sustain. Res. 2 (2021) 2000062, https://doi.org/10.1002/aesr.202000062.
- [14] T. Wang, et al., Enhancing oxygen reduction electrocatalysis by tuning interfacial hydrogen bonds, Nat. Catal. 4 (2021) 753–762, https://doi.org/10.1038/s41929-021-00668-0
- [15] Q. Wang, et al., Supported ionic liquid phase-boosted highly active and durable electrocatalysts towards hydrogen evolution reaction in acidic electrolyte, J. Energy Chem. 54 (2021) 342–351, https://doi.org/10.1016/j. jechem.2020.06.012.
- [16] H. Yang, et al., Metastable-phase platinum oxide for clarifying the Pt-O active site for the hydrogen evolution reaction, Energy Environ. Sci. 16 (2023) 574–583, https://doi.org/10.1039/D2EE03351H.
- [17] Z. Li, et al., A silver catalyst activated by stacking faults for the hydrogen evolution reaction, Nat. Catal. 2 (2019) 1107–1114, https://doi.org/10.1038/s41929-019-0365-0
- [18] C.E. Berdugo-Díaz, et al., Pathways for reactions of esters with H₂ over supported Pd catalysts: elementary steps, site requirements, and particle size effects, ACS Catal. 12 (2022) 9717–9734, https://doi.org/10.1021/acscatal.2c02129.
- [19] M. Munz, J. Poon, W. Frandsen, B.R. Cuenya, C.S. Kley, Nanoscale electron transfer variations at electrocatalyst–electrolyte interfaces resolved by in situ conductive atomic force microscopy, J. Am. Chem. Soc. 145 (2023) 5242–5251, https://doi. org/10.1021/jacs.2c12617.
- [20] B.Y. Tang, R.P. Bisbey, K.M. Lodaya, W.L. Toh, Y. Surendranath, Reaction environment impacts charge transfer but not chemical reaction steps in hydrogen evolution catalysis, Nat. Catal. 6 (2023) 339–350, https://doi.org/10.1038/ s41929-023-00943-2.
- [21] W. Sun, et al., Ultrathin aramid/COF heterolayered membrane for solid-state Limetal batteries, Nano Lett. 20 (2020) 8120–8126, https://doi.org/10.1021/acs.nanolett.0c03133.
- [22] S. Mitra, et al., Self-exfoliated guanidinium-based ionic covalent organic nanosheets (iCONs), J. Am. Chem. Soc. 138 (2016) 2823–2828, https://doi.org/ 10.1021/jacs.5b13533.
- [23] H. Lyu, C.S. Diercks, C. Zhu, O.M. Yaghi, Porous crystalline olefin-linked covalent organic frameworks, J. Am. Chem. Soc. 141 (2019) 6848–6852, https://doi.org/ 10.1021/jacs.9b02848.
- [24] L. Xiao, et al., Structural regulation of covalent organic frameworks for advanced electrocatalysis, Nano Energy 120 (2024) 109155, https://doi.org/10.1016/j. nanoen.2023.109155.
- [25] X. Cui, et al., Engineering organic polymers as emerging sustainable materials for powerful electrocatalysts, Chem. Soc. Rev. 53 (2024) 1447–1494, https://doi.org/ 10.1039/D3CS00727H
- [26] X. Cui, et al., Emerging covalent organic frameworks tailored materials for electrocatalysis, Nano Energy 70 (2020) 104525, https://doi.org/10.1016/j. nanoen.2020.104525.
- [27] D. Chen, et al., In situ preparation of thin and rigid COF film on Li anode as artificial solid electrolyte interphase layer resisting Li dendrite puncture, Adv. Funct. Mater. 30 (2020) 1907717, https://doi.org/10.1002/adfm.201907717.
- [28] N. Huang, P. Wang, D. Jiang, Covalent organic frameworks: a materials platform for structural and functional designs, Nat. Rev. Mater. 1 (2016) 16068, https://doi. org/10.1038/natrevmats.2016.68.
- [29] S. Kandambeth, et al., Construction of crystalline 2D covalent organic frameworks with remarkable chemical (acid/base) stability via a combined reversible and irreversible route, J. Am. Chem. Soc. 134 (2012) 19524–19527, https://doi.org/ 10.1021/ja308278w.
- [30] C. Li, et al., Covalent organic frameworks with high quantum efficiency in sacrificial photocatalytic hydrogen evolution, Nat. Commun. 13 (2022) 2357, https://doi.org/10.1038/s41467-022-30035-x.
- [31] Z. Li, et al., Three-component donor–π–acceptor covalent–organic frameworks for boosting photocatalytic hydrogen evolution, J. Am. Chem. Soc. 145 (2023) 8364–8374, https://doi.org/10.1021/jacs.2c11893.
- [32] T. He, et al., Integrated interfacial design of covalent organic framework photocatalysts to promote hydrogen evolution from water, Nat. Commun. 14 (2023) 329, https://doi.org/10.1038/s41467-023-35999-y.
- [33] G. Kresse, J. Hafner, Ab initio molecular dynamics for open-shell transition metals, Phys. Rev. B 48 (1993) 13115–13118, https://doi.org/10.1103/ PhysRevB.48.13115.

- [34] J.P. Perdew, K. Burke, M. Ernzerhof, Generalized gradient approximation made simple, Phys. Rev. Lett. 77 (1996) 3865–3868, https://doi.org/10.1103/ PhysRevLett 77 3865
- [35] P.E. Blöchl, Projector augmented-wave method, Phys. Rev. B 50 (1994) 17953–17979, https://doi.org/10.1103/PhysRevB.50.17953.
- [36] H.J. Monkhorst, J.D. Pack, Special points for Brillouin-zone integrations, Phys. Rev. B 13 (1976) 5188–5192, https://doi.org/10.1103/PhysRevB.13.5188.
- [37] J. Hussain, H. Jónsson, E. Skúlason, Faraday efficiency and mechanism of electrochemical surface reactions: CO₂ reduction and H₂ formation on Pt(111), Faraday Discuss. 195 (2016) 619–636, https://doi.org/10.1039/C6FD00114A.
- [38] G. Henkelman, B.P. Uberuaga, H. Jónsson, A climbing image nudged elastic band method for finding saddle points and minimum energy paths, J. Chem. Phys. 113 (2000) 9901–9904, https://doi.org/10.1063/1.1329672.
- [39] S. Choi, J. Park, K. Kwak, M. Cho, Substituent effects on the vibrational properties of the CN stretch mode of aromatic nitriles: IR probes useful for time-resolved IR spectroscopy, Chem. Asian J. 16 (2021) 2626–2632, https://doi.org/10.1002/ asia.202100657.
- [40] J. Ma, et al., Solid-state NMR study of adsorbed water molecules in covalent organic framework materials, Microporous Mesoporous Mater. 305 (2020) 110287, https://doi.org/10.1016/j.micromeso.2020.110287.
- [41] G. Zhang, et al., Accumulation of glassy poly(ethylene oxide) anchored in a covalent organic framework as a solid-state Li⁺ electrolyte (https://doi.org./), J. Am. Chem. Soc. 141 (2019) 1227–1234, https://doi.org/10.1021/jacs.8b0767(
- [42] Y. He, W.F. Chen, W.B. Yu, G. Ouyang, G.W. Yang, Anomalous interface adhesion of graphene membranes, Sci. Rep. 3 (2013) 2660, https://doi.org/10.1038/ sren02660
- [43] D.S. Silvester, et al., Electrical double layer structure in ionic liquids and its importance for supercapacitor, battery, sensing, and lubrication applications, J. Phys. Chem. C 125 (2021) 13707–13720, https://doi.org/10.1021/acs. jpcc.1c03253.
- [44] S.-J. Shin, et al., On the importance of the electric double layer structure in aqueous electrocatalysis, Nat. Commun. 13 (2022) 174, https://doi.org/10.1038/ s41467-021-27909-x.
- [45] T. Shinagawa, A.T. Garcia-Esparza, K. Takanabe, Insight on Tafel slopes from a microkinetic analysis of aqueous electrocatalysis for energy conversion, Sci. Rep. 5 (2015) 13801, https://doi.org/10.1038/srep13801.
- [46] Z.-C. Guo, Z.-Q. Shi, X.-Y. Wang, Z.-F. Li, G. Li, Proton conductive covalent organic frameworks, Coord. Chem. Rev. 422 (2020) 213465, https://doi.org/10.1016/j. ccr.2020.213465.
- [47] S. Chandra, et al., Interplaying intrinsic and extrinsic proton conductivities in covalent organic frameworks, Chem. Mater. 28 (2016) 1489–1494, https://doi. org/10.1021/acs.chemmater.5b04947.
- [48] Y. Li, et al., Fabrication of Nafion/zwitterion-functionalized covalent organic framework composite membranes with improved proton conductivity, J. Membr. Sci. 568 (2018) 1–9. https://doi.org/10.1016/j.memsci.2018.09.050.
- [49] K. Kodama, et al., Catalyst poisoning property of sulfonimide acid ionomer on Pt (111) surface, J. Electrochem. Soc. 161 (2014) F649–F652, https://doi.org/ 10.1149/2.051405ies
- [50] K. Kodama, et al., Increase in adsorptivity of sulfonate anions on Pt (111) surface with drying of ionomer, Electrochem. Comm. 36 (2013) 26–28, https://doi.org/ 10.1016/j.elecom.2013.09.005.
- [51] J.W. Peck, D.I. Mahon, D.E. Beck, B.E. Koel, TPD study of the adsorption and reaction of nitromethane and methyl nitrite on ordered Pt–Sn surface alloys, Surf. Sci. 410 (1998) 170–188, https://doi.org/10.1016/S0039-6028(98)00198-8.
- [52] J. Kim, B. Song, I. Chung, J. Park, Y. Yun, High-performance Pt catalysts supported on amine-functionalized silica for enantioselective hydrogenation of α-keto ester, J. Catal. 396 (2021) 81–91, https://doi.org/10.1016/j.jcat.2021.02.001.
- [53] E. Skúlason, et al., A theoretical evaluation of possible transition metal electrocatalysts for N₂ reduction, Phys. Chem. Chem. Phys. 14 (2012) 1235–1245, https://doi.org/10.1039/C1CP22271F.



Jung Hyun Park is a Visiting Senior Scientific Specialist at the Illinois Sustainable Technology Center at the University of Illinois at Urbana-Champaign. He received his PhD in Chemical Engineering from Hanyang University in 2020. In 2021, he joined UIUC as a post-doctoral research fellow with support from the Korean National Research Foundation, which awarded him a Postdoctoral Fellowship. His research interests include catalyst material development and surface modification for electrochemical, thermochemical, and photochemical catalysis applications aimed at addressing sustainable energy and environmental issues.



Chi Ho Lee is a post-doctoral researcher of Artie McFerrin Department of Chemical Engineering at Texas A&M University. He earned his Ph.D. in Bionano technology from Hanyang University, where he specialized in developing electrocatalysts for energy applications. In particular, his research integrates density functional theory (DFT), kinetic Monte Carlo (kMC), and machine learning (ML) to advance theoretical methodologies in this field.



Siying Yu received her B.Sc. degree in Chemistry from Peking University in 2019. She then joined Professor Hong Yang's group at the University of Illinois at Urbana-Champaign (UIUC) as a Ph.D. student in the same year. Her graduate research has focused on the development and characterization of low-PGM electrocatalysts for fuel cell applications, non-precious metal catalysts for water electrolysis and thermal catalysis.



Priti Kharel received her Bachelor's degree in Chemistry from Hamilton College in 2018. She then joined University of Illinois at Urbana-Champaign to pursue her PhD under the supervision of Prof. Pinshane Huang. Her thesis research focuses on developing advanced electron microscopy techniques to image 2D molecular crystals at the angstrom-scale.



Pinshane Y. Huang is an Associate Professor and Racheff Faculty Scholar in the Department of Materials Science and Engineering at the University of Illinois at Urbana-Champaign, where she is also the Associate Director of the Materials Research Laboratory. Pinshane holds a Ph.D. in Applied and Engineering Physics from Cornell University and B.A in Physics from Carleton College. Her research focuses on transmission electron microscopy of two-dimensional and nanoelectronic materials. Her awards include a Presidential Early Career Award for Scientists and Engineers (PECASE), a Packard Fellowship, a Sloan Fellowship, as well as Air Force Young Investigator and NSF CAREER awards.



Joseph Sang-Il Kwon is an associate professor of Artie McFerrin Department of Chemical Engineering at Texas A&M University. He earned his Ph.D. in Chemical Engineering from University of California, Los Angeles. His work is driven by the goal of merging fundamental engineering principles, data analysis, efficient model reduction, parameter estimation, machine learning, and optimization-based control algorithms to gain a deeper understanding of complex systems and develop innovative solutions that can have a significant impact on the industrial sector.



Hong Yang is the Richard C. Alkire Chair Professor in Chemical Engineering at UIUC. He received his Ph.D. degree in 1998 from University of Toronto and did his postdoctoral training as an NSERC Postdoctoral Fellow at Harvard University. He worked at University of Rochester between 2001 and 2011 and moved to UIUC in 2012. He is an elected Fellow of AAAS, the winner of the Doctoral Prize from NSERC Canada, and the recipient of the CAREER Award from US NSF. His current research interests are on the material chemistry approach to the development of nanostructures for catalysis, energy, and sustainability applications.

Supporting Information

Effects of amine-based covalent organic framework on platinum electrocatalyst performance towards hydrogen evolution reaction

Jung Hyun Park,^{a,1,2} Chi Ho Lee,^{b,c,1} Siying Yu,^a Priti Kharel,^d Roady Choi,^a Cheng Zhang,^a Pinshane Y. Huang,^e Joseph Sang-Il Kwon,^{b,c,*} Hong Yang^{a,d,*}

^a Department of Chemical and Biomolecular Engineering, University of Illinois at Urbana-Champaign, 600 South Mathews Avenue, Urbana, IL 61801, United States

^b Artie McFerrin Department of Chemical Engineering, Texas A&M University, College Station, TX 77843, United States

^c Texas A&M Energy Institute, College Station, TX 77843, United States

^d Department of Chemistry, University of Illinois at Urbana-Champaign, Urbana, IL 61801, United States

^e Department of Materials Science and Engineering, University of Illinois at Urbana-Champaign, Urbana, IL 61801, United States

¹These authors contributed equally to this work.

²Current address: Illinois Sustainable Technology Center, University of Illinois at Urbana-Champaign, 1 Hazelwood Drive, Champaign, IL 61820, United States.

*Correspondence to: hy66@illinois.edu (HY), kwonx075@tamu.edu (JSK)

Keywords: covalent organic framework, hydrogen evolution reaction, electrocatalysis, HER, solid-liquid interface model.

Notes for Computational Analysis of Hydrogen Evolution Reaction Mechanisms

Hydrogen evolution reaction (HER) potential analysis based on TCM-CHE approach. On simulation studies, we used the free energy diagram (FED) based on the thermochemical model (TCM) and computational hydrogen electrode (CHE)¹ to calculate the free energy for electrochemical reactions. This is the preferred density functional theory (DFT) method for studying the electrochemical reactions. In this simulation framework, chemical potential of proton and electron pair ($\mu(H^+ + e^-)$) is estimated from the half of chemical potential of H_2 gas at pH equal to zero, and it can be shifted by -eU when the external potential U is applied, i.e., $\mu(H^+ + e^-) = 0.5\mu(H_2) - eU$. For the investigation of catalytic reactions on a specific surface, thermodynamic stability of the adsorbent is considered as the main descriptor, which is used to determine the rate-limiting step (RLS). For HER, generation of H_2 generally follows either Volmer-Tafel or Volmer-Heyrovsky mechanism in the following steps:

Volmer reaction:
$$2H^+ + 2e^- \rightarrow H^* + H^+ + e^-$$
 (1)

Tafel reaction:
$$H^* + H^* \rightarrow H_2 + *$$
 (2)

Heyrovsky reaction:
$$H^* + H^+ \rightarrow H_2 + *$$
 (3)

where * and H* are the active site and adsorbed H atom on the catalyst surface, respectively. In this study, the chemical potentials of the initial $(2H^+ + 2e^-)$ and final states (H_2) are the same, since the equilibrium reduction potential for the HER is 0 V. Thus, their intermediate states should have the same chemical potential as the initial and final states under equilibrium potential for an ideal catalyst, that is, U equals to 0 V. However, the actual catalyst deviates from the ideal case due to the binding strength of the intermediate on catalyst surface. Therefore, the optimum value of Gibbs free energy of the intermediate (H^*) should be zero for a spontaneous reaction without a barrier.

To investigate the free energy between elementary steps, including proton and electron transfer, we obtain the potential under the standard condition (298.15 K and 1 atm). Here, ΔG value of an elementary step in HER can be obtained using the following equation:

$$\Delta G = \Delta E + \Delta E_{ZPE} - T\Delta S + \Delta G_{U} + \Delta G_{pH}$$
 (4)

where ΔE is the binding energy of adsorbent, T is the absolute temperature, ΔE_{ZPE} is the change in the zero-point energy, and ΔS is the change in entropy. The value of E_{ZPE} and S can be computed from the vibrational frequency values of the adsorbed species, which are

obtained from finite-difference calculations. ΔG_{pH} is the contribution of H⁺, which can be determined as the product of $\kappa_B T * \ln(10) * pH$, where κ_B is the Boltzmann constant. ΔG_U can be used to evaluate the effect of the applied bias at electrode, which is equal to – neU, where n is the number of transferred electrons in each step. Thus, we used limiting potential (U_L) to assess the catalytic activity that can be determined by:

$$U_{L} = -\max(\Delta G_{1}, \Delta G_{2}, \Delta G_{3}, \dots, \Delta G_{i})/e$$
 (5)

where ΔG_i is the reaction free energy between elementary steps in the overall HER.

HER rate analysis based on the ESLI model. Although the TCM-CHE approach described above can be quite successful in the prediction of HER overpotential by finding potential-determining step (PDS),¹ the reaction rate cannot be properly analysed by this approach when catalyst surface, COF, proton, and near surface water molecules must be considered. Hence, we constructed a different model, the so-called electrochemical solid-liquid interface (ESLI), which is comprised of a metal catalyst surface, additional electrons in the metal, and solvated protons in water layer above the surface.² This ESLI model allows to study the effect of solvation and electrode potential by explicitly varying the proton-electron concentration at the interface. To mimic an acidic environment for HER and calculate the overpotential, we added a proton in the water double layer outside the surfaces of interests (*i.e.*, Pt, Bz-COF, NH₂-COF, SO₃-COF, and NO₂-COF). Based on these interfacial structures, we calculated the electrode potentials.

In addition, we calculated the energy barriers for proton-electron transfer to determine rates for all elementary steps under a predetermined external potential to the surface, and applied the corresponding, calculated reaction energy barriers to the free energy diagram (FED), which was obtained by the TCM-CHE approach. The rate-limiting step (RLS) was determined based on the reconstructed FED and used to verify the preferred reaction pathway from adsorption of H to desorption of H_2 gas. Specifically, in the case of H_2 gas desorption step, only the Tafel reaction was considered based on the experimental observation that Tafel slopes for the COF-modified electrocatalysts were $\sim 30 \text{ mV/dec}$.

Figures

Fig. S1. Synthetic route of COFs by the Schiff-base reaction using triformylphloroglucinol (TPG), different diamine compounds and other additives.

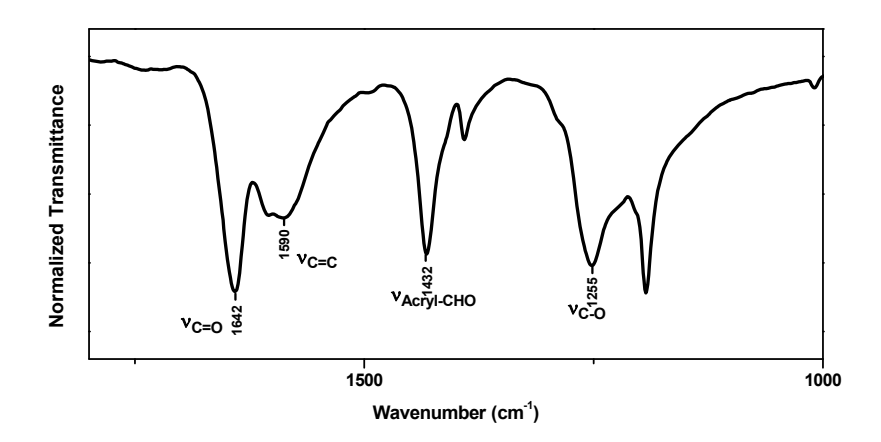


Fig. S2. FT-IR spectrum for TPG.

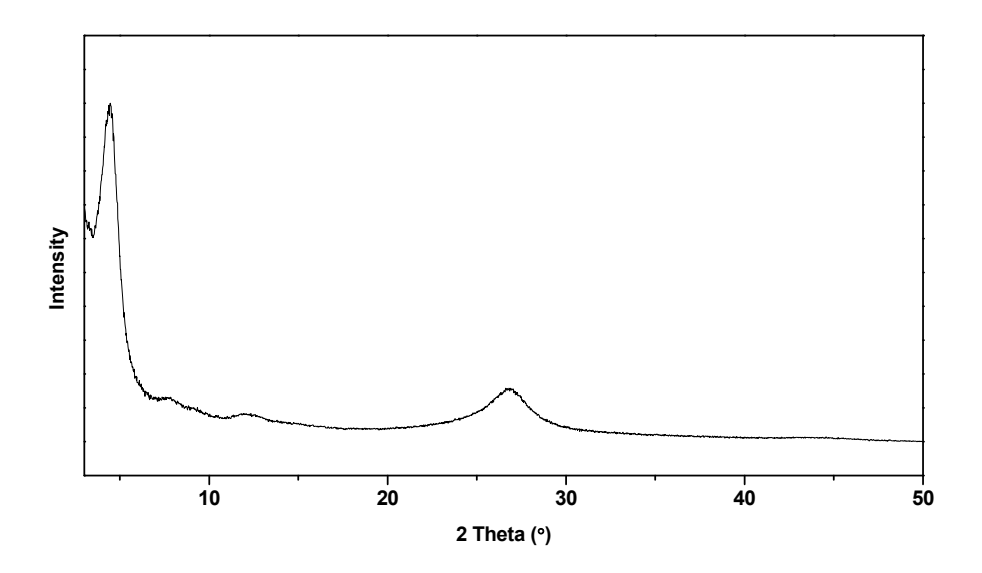


Fig. S3. Powder XRD pattern for NO₂-COF.

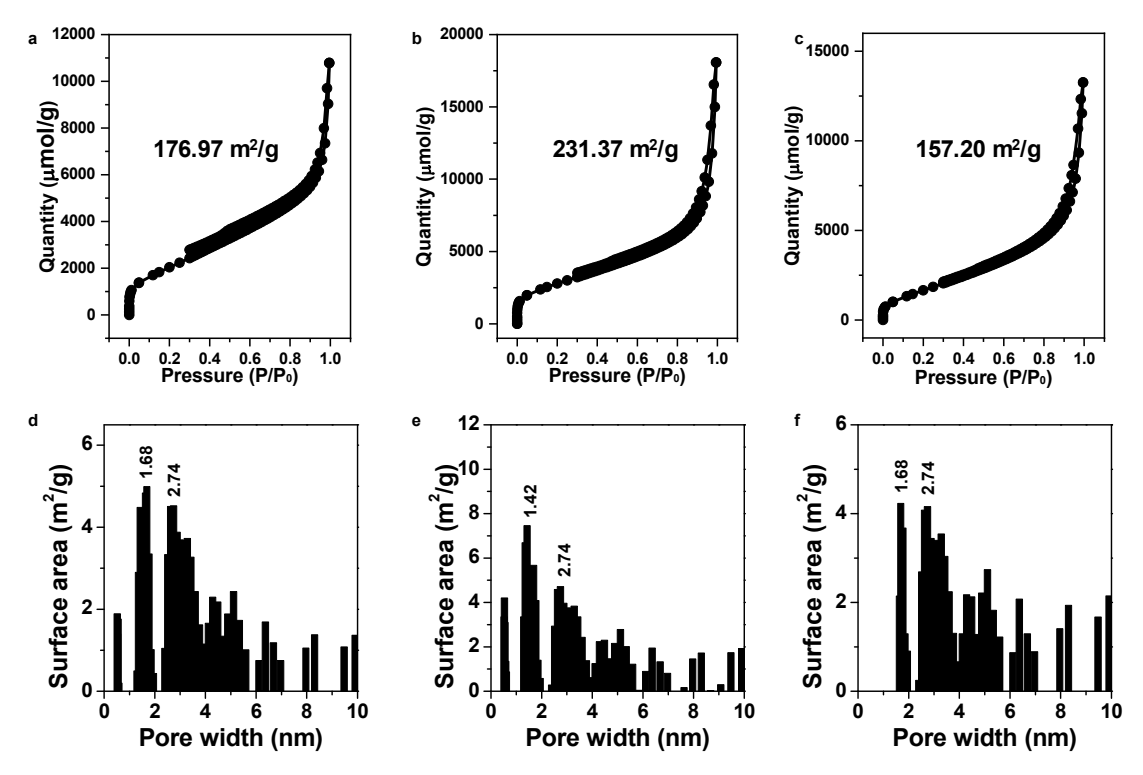


Fig. S4. N₂ adsorption-desorption isotherm of (a) Bz-COF, (b) NH₂-COF, (c) SO₃-COF and the corresponding pore size distribution analyses of (d) Bz-COF, (e) NH₂-COF, and (f) SO₃-COF based on the NL-DFT model.

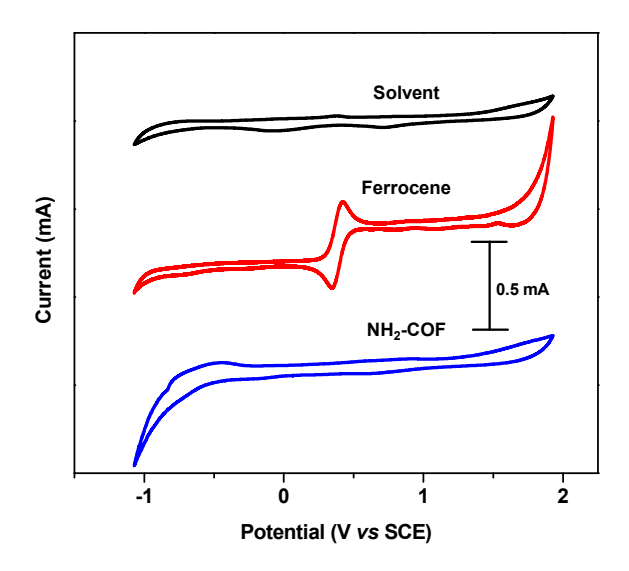


Fig. S5. Cyclic voltammograms for as-prepared NH₂-COF, tested in 0.2 M tetrabutylammonium perchlorate in acetonitrile.

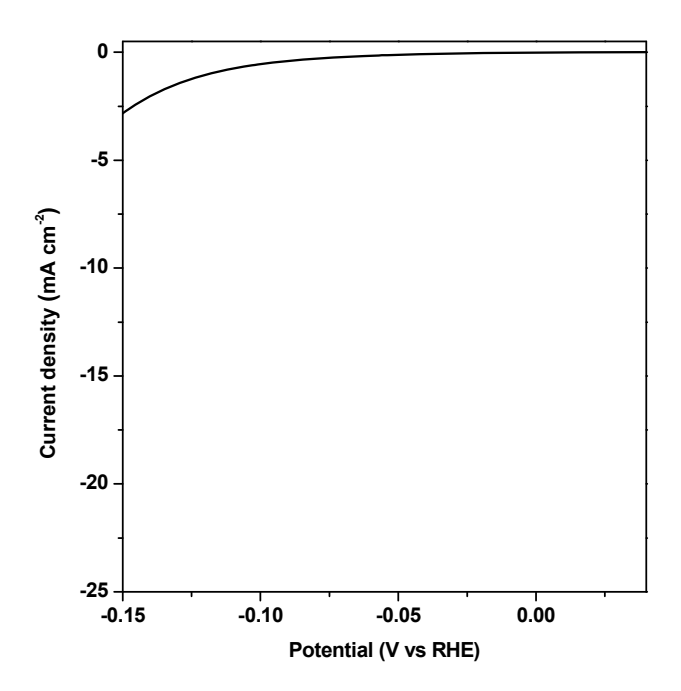


Fig. S6. Linear sweep voltammogram for HER using only NH2-COF.

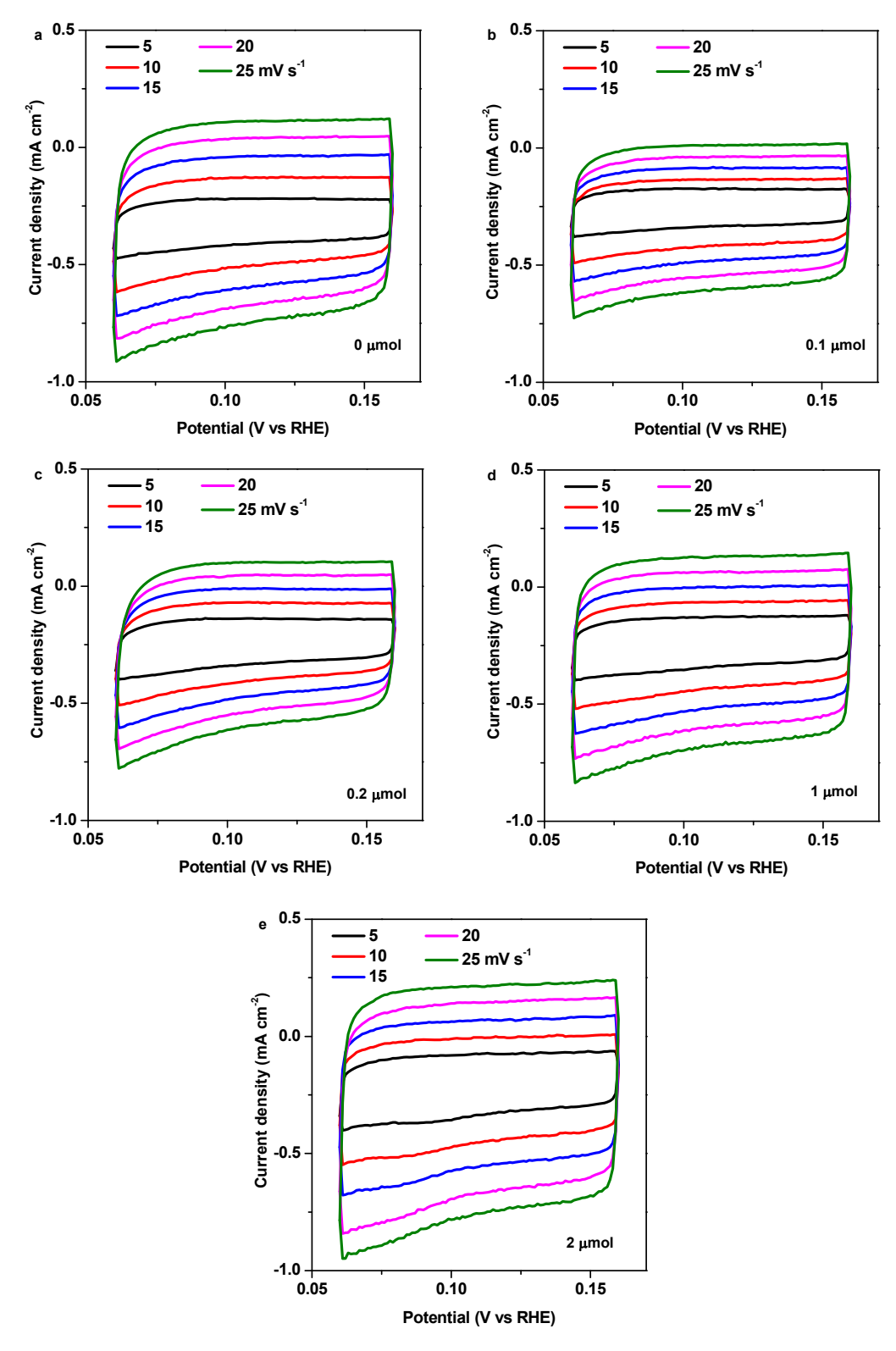


Fig. S7. Cyclic voltammograms of Pt electrocatalysts modified with (a) 0 (pristine Pt), (b) 0.1, (c) 0.2, (d) 1, and (e) 2 μ mol of NH₂-COF, respectively.

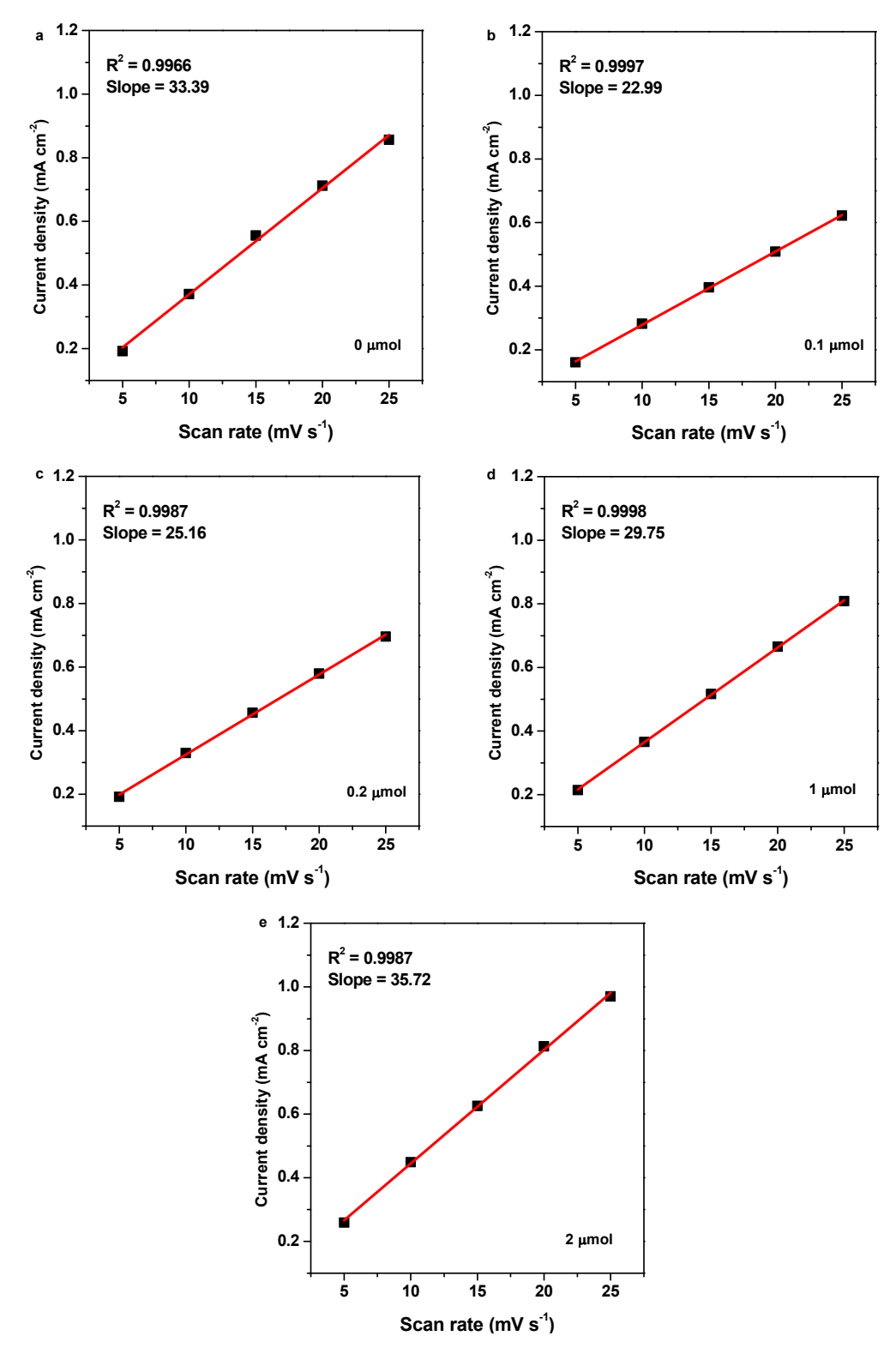


Fig. S8. Difference in current density (J_a-J_c) between anode (J_a) and cathode (J_c) at 0.11 V (vs. RHE) as a function of scan rate for Pt electrocatalysts modified with (a) 0 (Pt only), (b) 0.1, (c) 0.2, (d) 1, and (e) 2 μ mol of NH₂-COF, respectively.

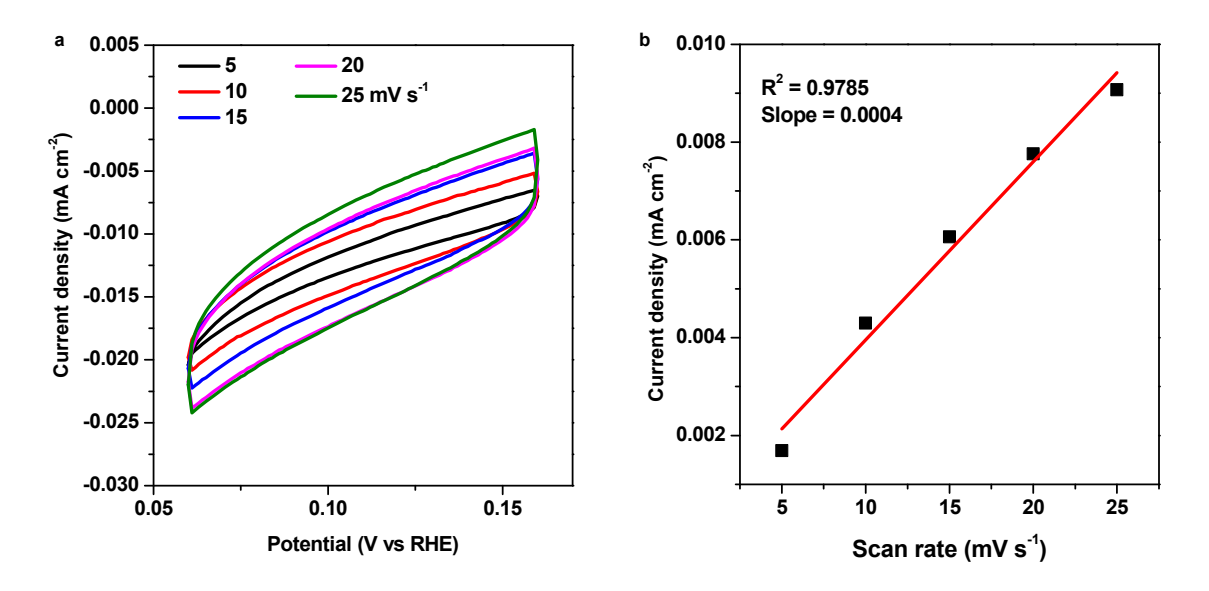


Fig. S9. (a) Cyclic voltammograms and (b) difference between anode (J_a) and cathode (J_c) in current density (J_a - J_c) at 0.11 V (vs. RHE) as a function of scan rate for NH₂-COF only.

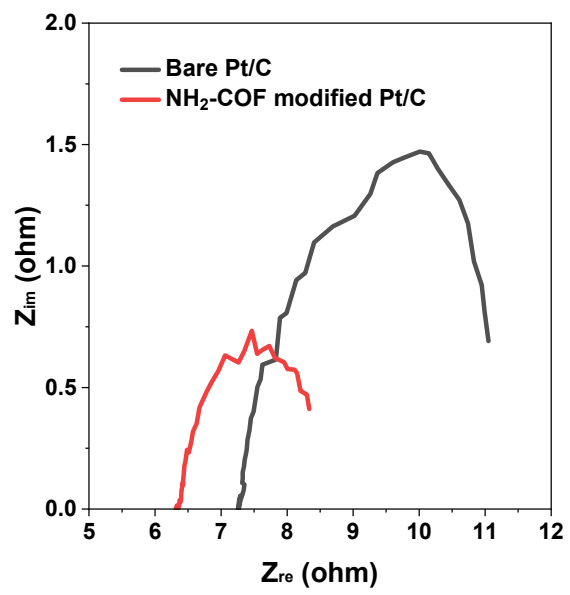


Fig. S10. Nyquist plots of bare Pt/C and NH₂-COF modified Pt/C at -0.02 V (vs. RHE) using impedance spectroscopy.

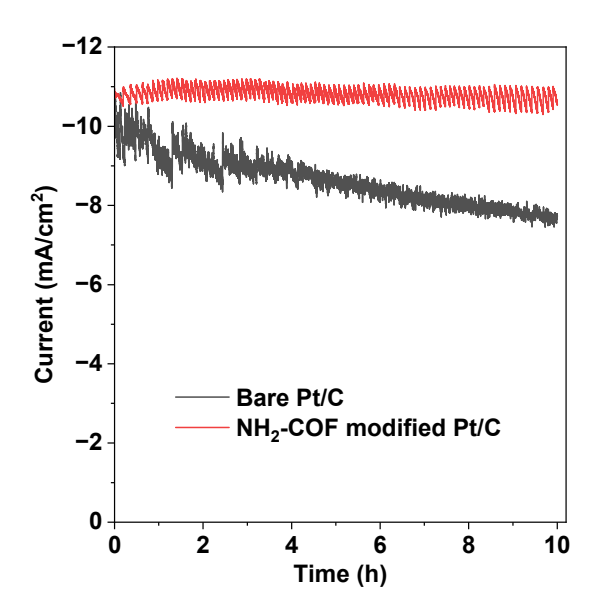


Fig. S11. Chronoamperometry studies of bare and NH₂-COF modified Pt/C electrocatalysts at -0.02 V (vs. RHE). The concentration of NH₂-COF used in the synthesis was 2 μ mol.

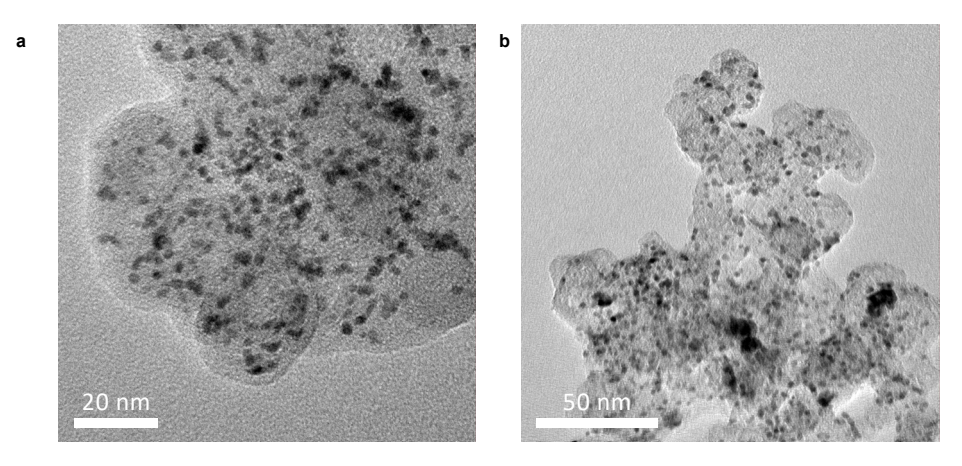


Fig. S12. TEM images of the NH₂-COF modified Pt/C electrocatalyst (a) before and (b) after the stability test.

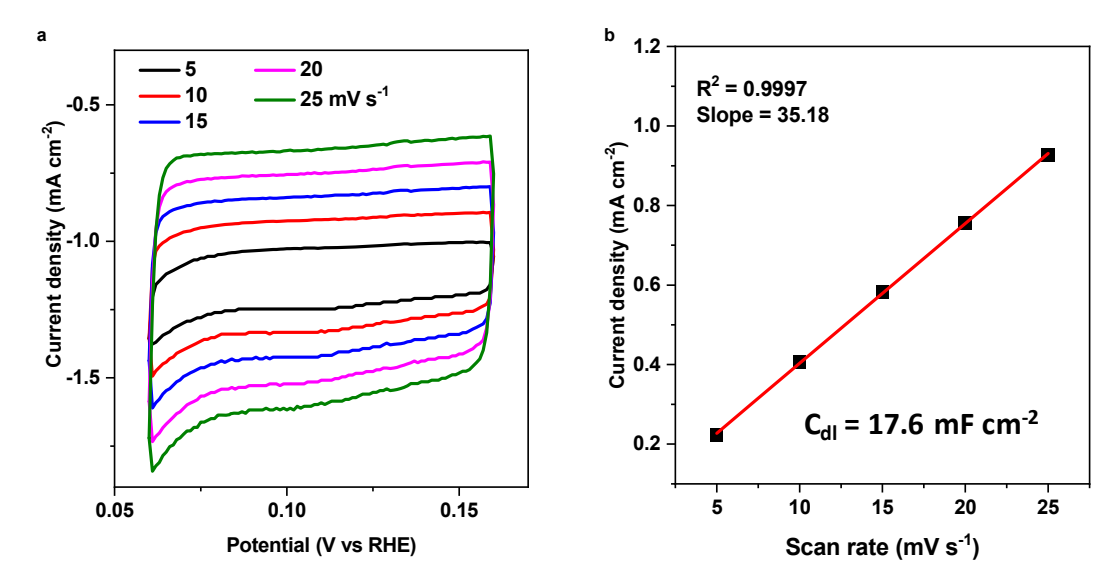


Fig. S13. Double layer capacitance (C_{dl}) measurement. (a) Cyclic voltammograms and (b) difference in current density (J_a - J_c) between anode (J_a) and cathode (J_c) at 0.11 V (vs. RHE) as a function of scan rate of Pt/C electrocatalysts modified with 2 µmol of NH₂-COF after the stability test.

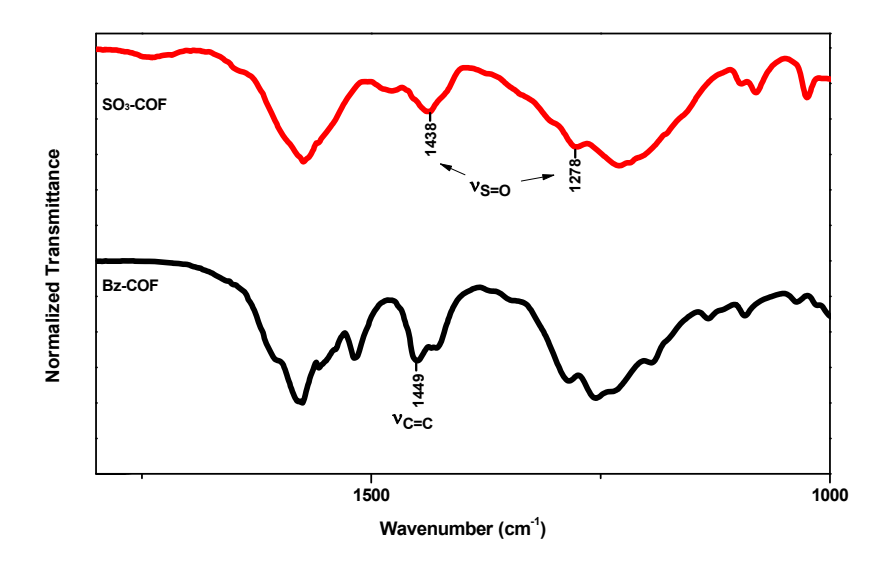


Fig. S14. FT-IR spectra of Bz-COF (black) and SO₃-COF (red).

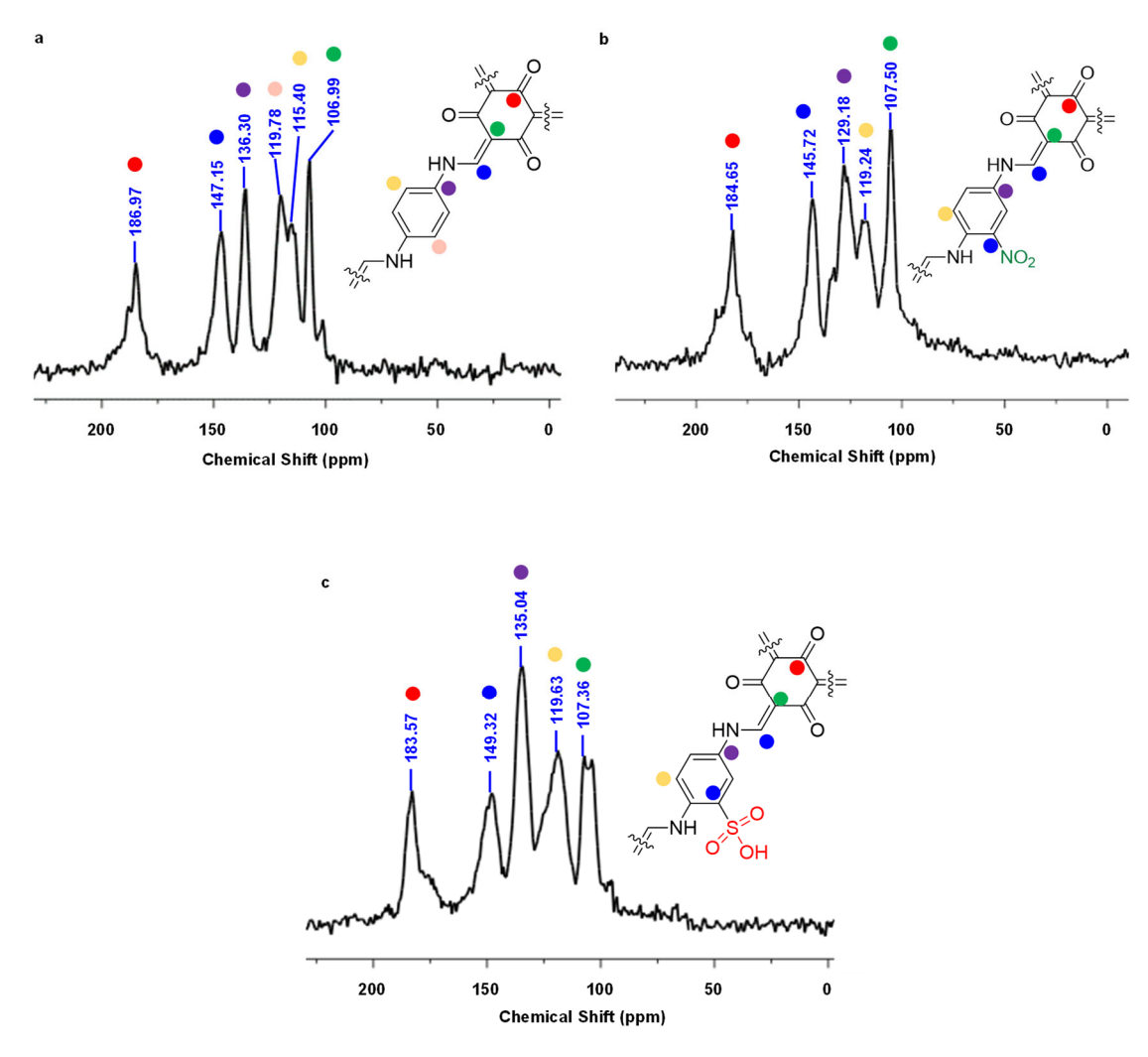


Fig. S15. Solid-state ¹³C NMR spectra for (a) Bz-COF, (b) NO₂-COF, and (c) SO₃-COF.

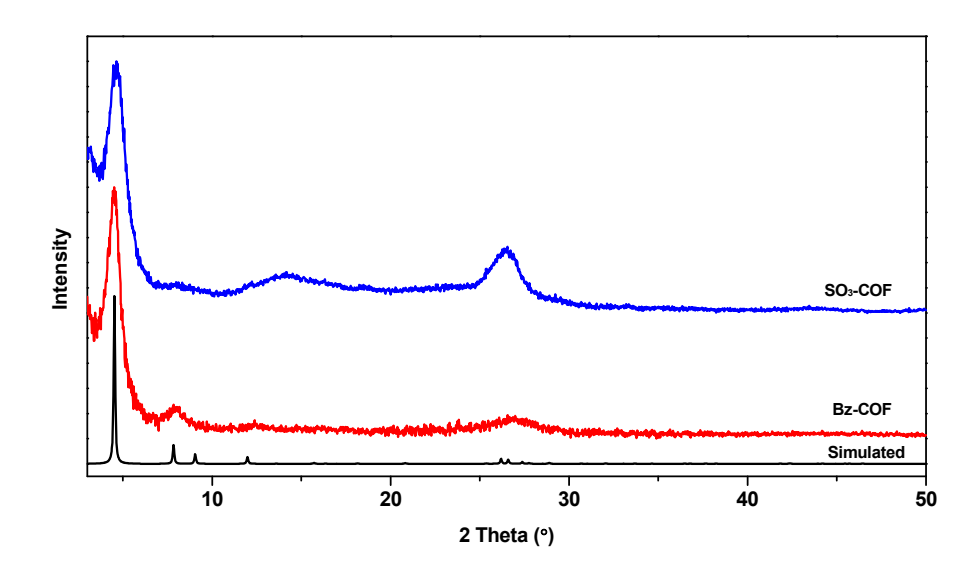


Fig. S16. Powder XRD patterns for Bz-COF (red) and SO₃-COF (blue), together with the simulated XRD for Bz-COF (black).

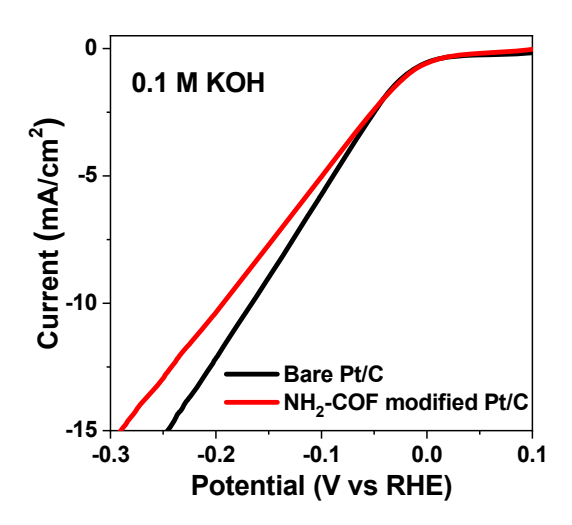


Fig. S17. LSV polarization curves for HER catalyzed by the Pt/C electrocatalysts with and without the modification by NH₂-COF (2 μ mol) in 0.1 M KOH electrolyte.

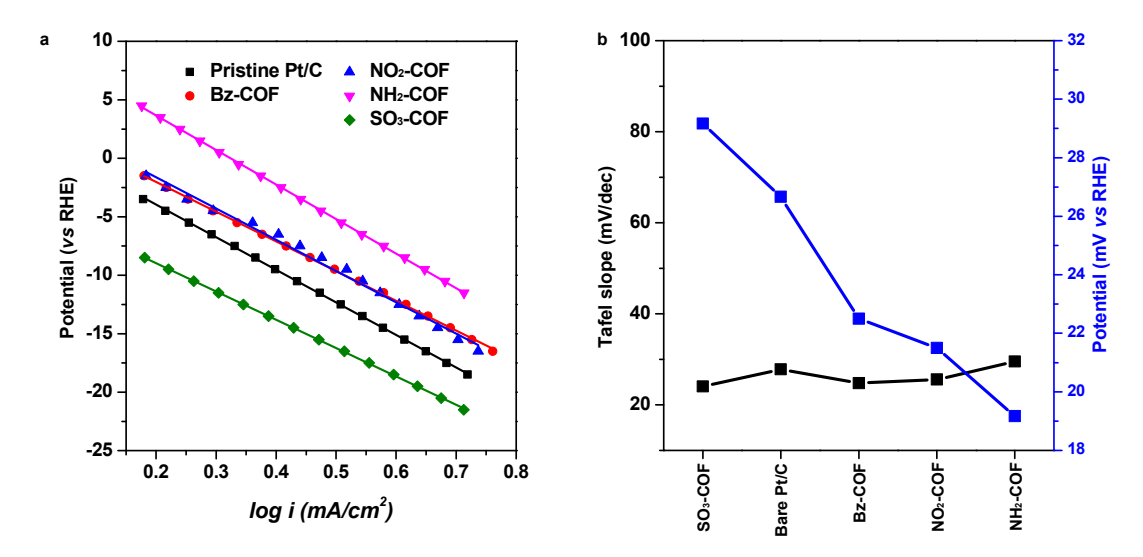


Fig. S18. (a) Tafel slopes and (b) their relationship with overpotentials for Pt electrocatalysts modified with different COFs (2 μ mol).

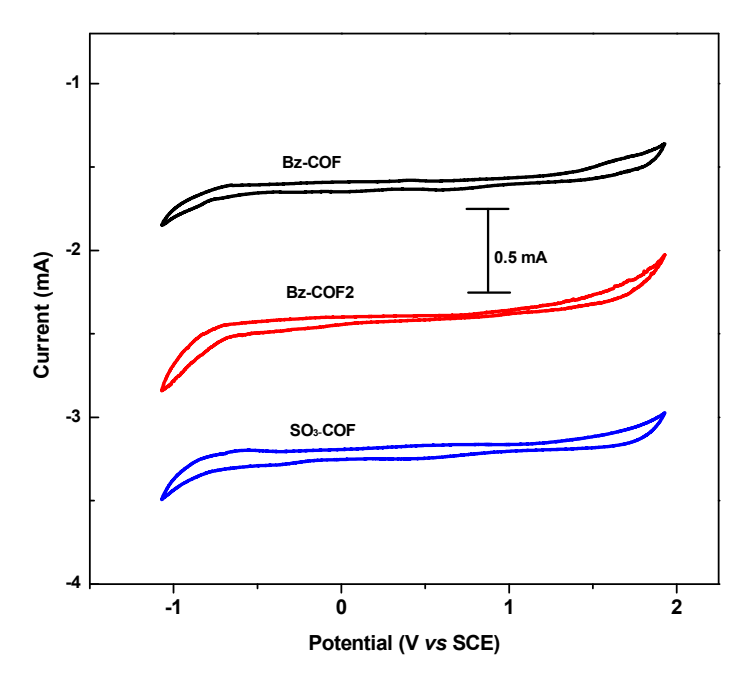


Fig. S19. Cyclic voltammogram for Bz-COF (black), Bz-COF2 (red), and SO₃-COF (blue).

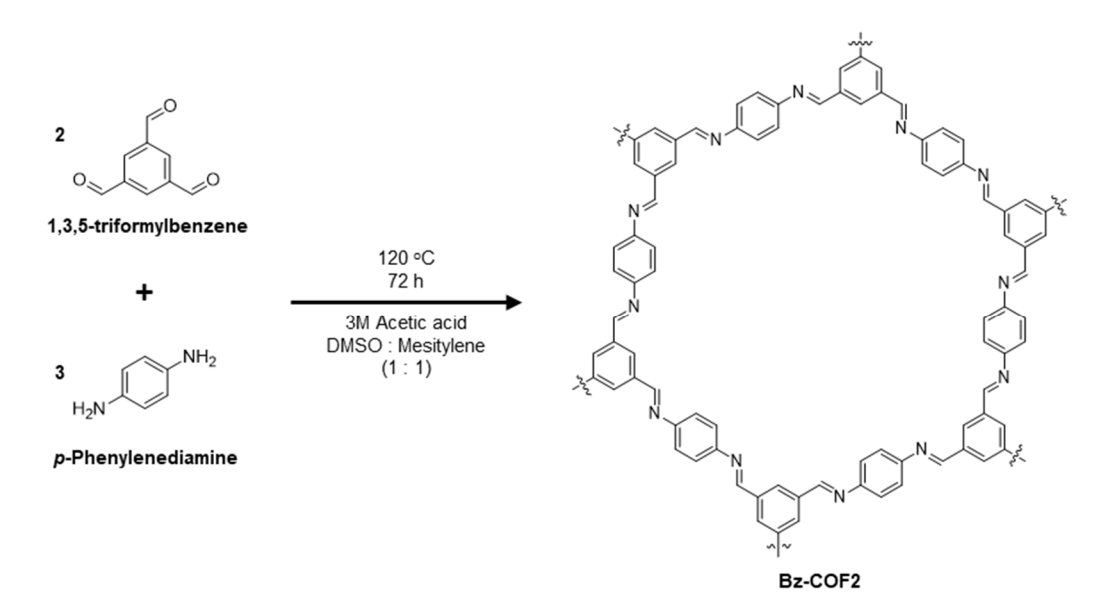


Fig. S20. Reaction for making Bz-COF2 using Schiff-base reaction between 1,3,5-triformylbenzene and *p*-phenylenediamine.

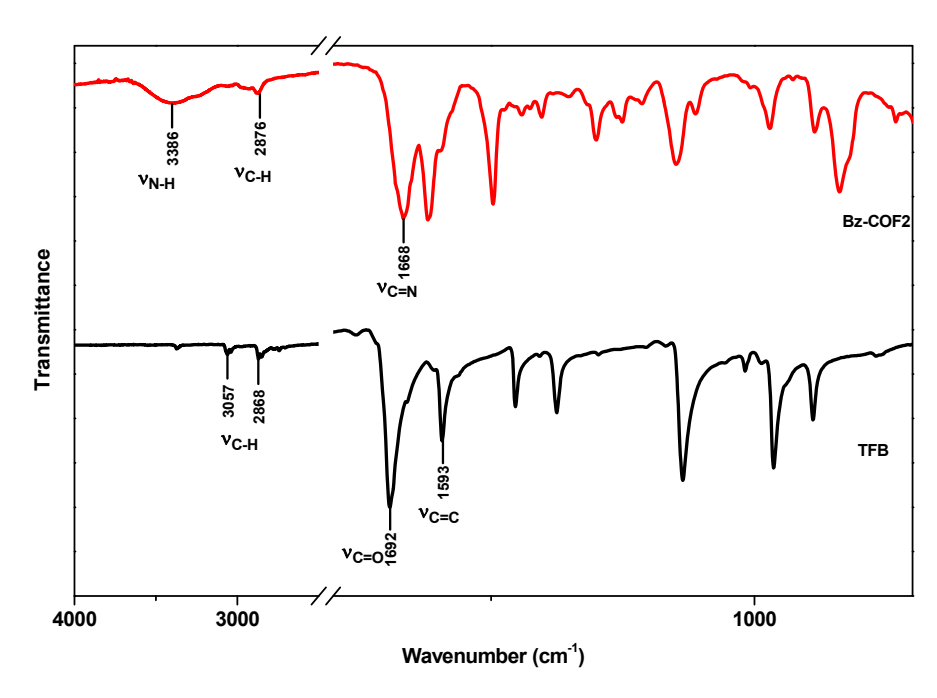


Fig. S21. FT-IR spectra for 1,3,5-triformylbenzene (TFB, black) and Bz-COF2 (red).

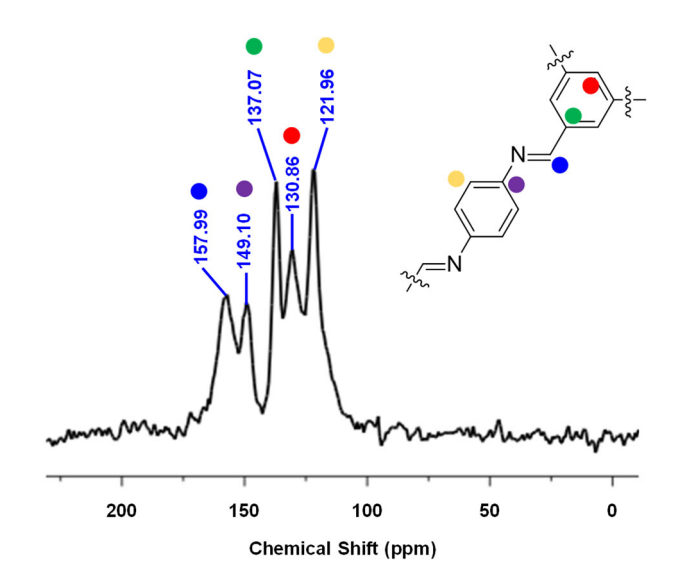


Fig. S22. Solid-state ¹³C NMR spectrum for Bz-COF2.

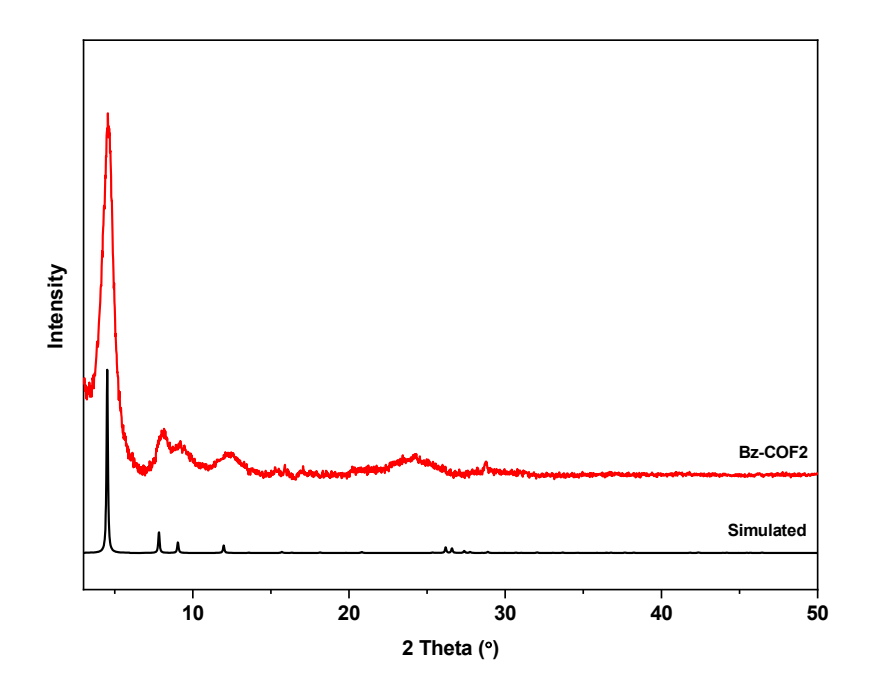


Fig. S23. Powder XRD patterns for simulated Bz-COF (black) and experimentally determined Bz-COF2 (red).

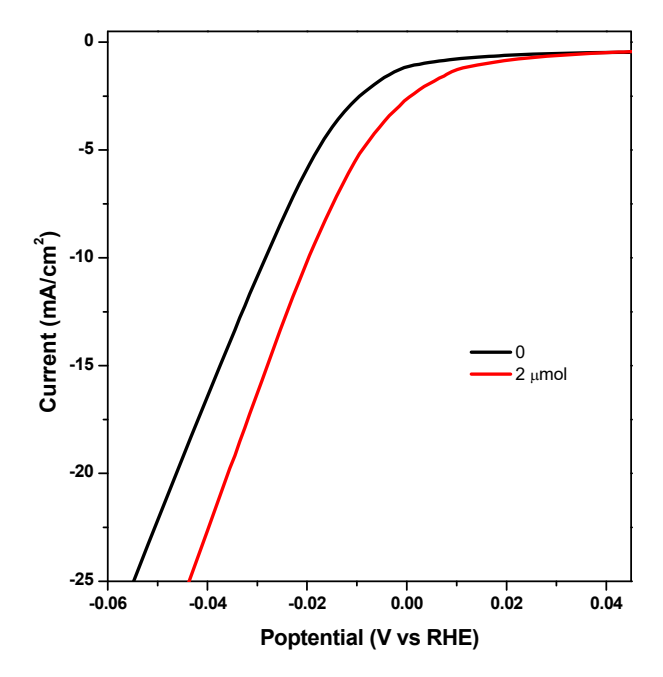


Fig. S24. Linear sweep voltammograms for HER of the Pt electrocatalysts with and without the modification by Bz-COF2.

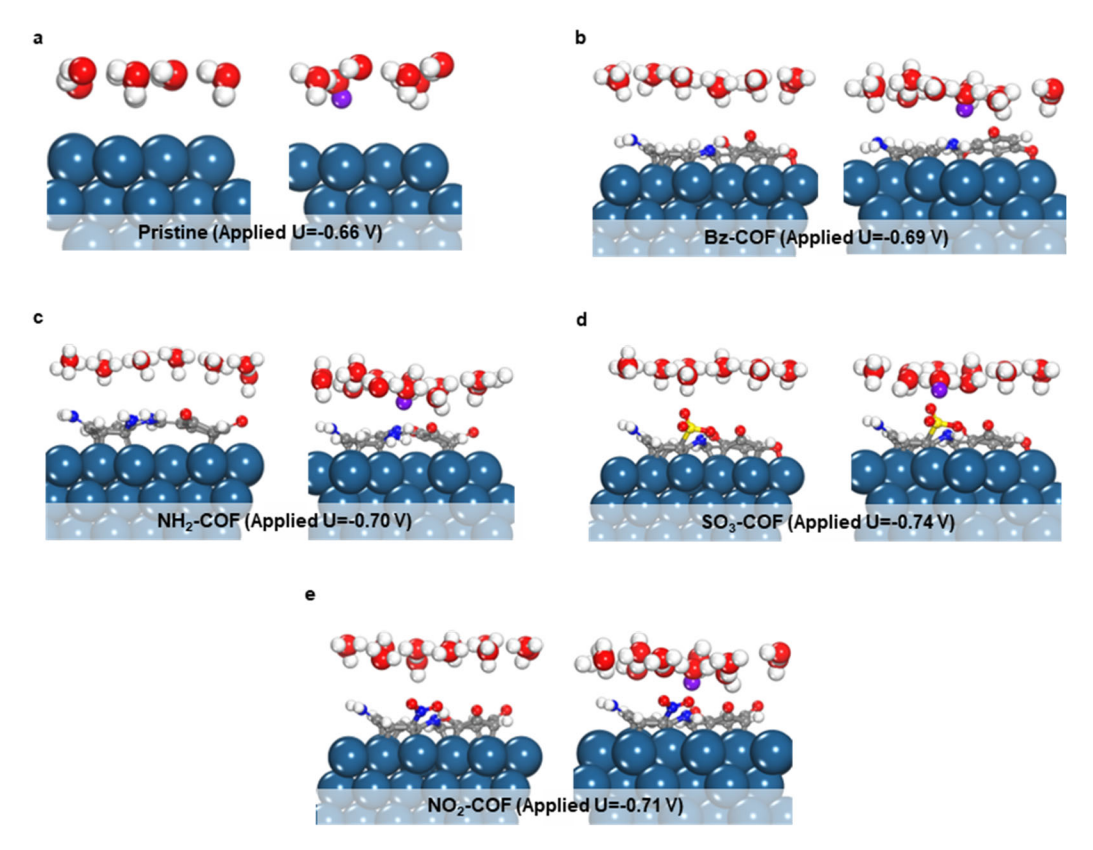


Fig. S25. Side views of the computational models used in the study. The electrocatalysts are made of COF-modified Pt covered by a bilayer of water without (left) or with (right) a hydronium ion (H₃O⁺): (a) no COF, (b) Bz-COF, (c) NH₂-COF, (d) SO₃-COF, and (e) NO₂-COF structures. The optimized surface potentials are -0.66 V for Pt, -0.69 V for Bz-COF modified Pt, -0.70 V for NH₂-COF modified Pt, -0.74 V for SO₃-COF modified Pt, and -0.71 V for NO₂-COF modified Pt. Color code: dark blue, Pt; bright blue, N; red, O; gray, C; white: H; yellow, S; and purple, H⁺ (in H₃O⁺).

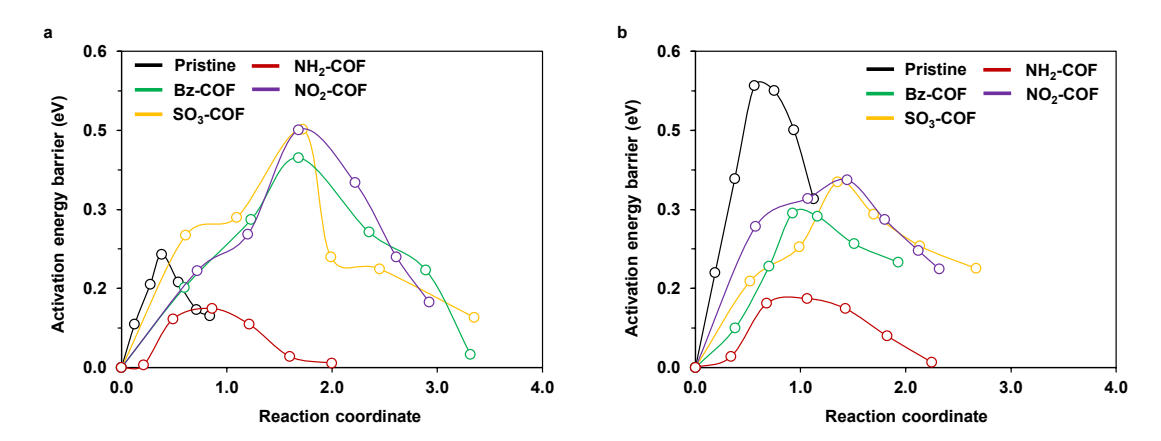


Fig. S26. Activation energy calculations of (a) first and (b) second Volmer step for the Pt electrocatalysts modified by different COFs: pristine (black), Bz-COF (green), NH₂-COF (red), NO₂-COF (purple), and SO₃-COF (yellow).

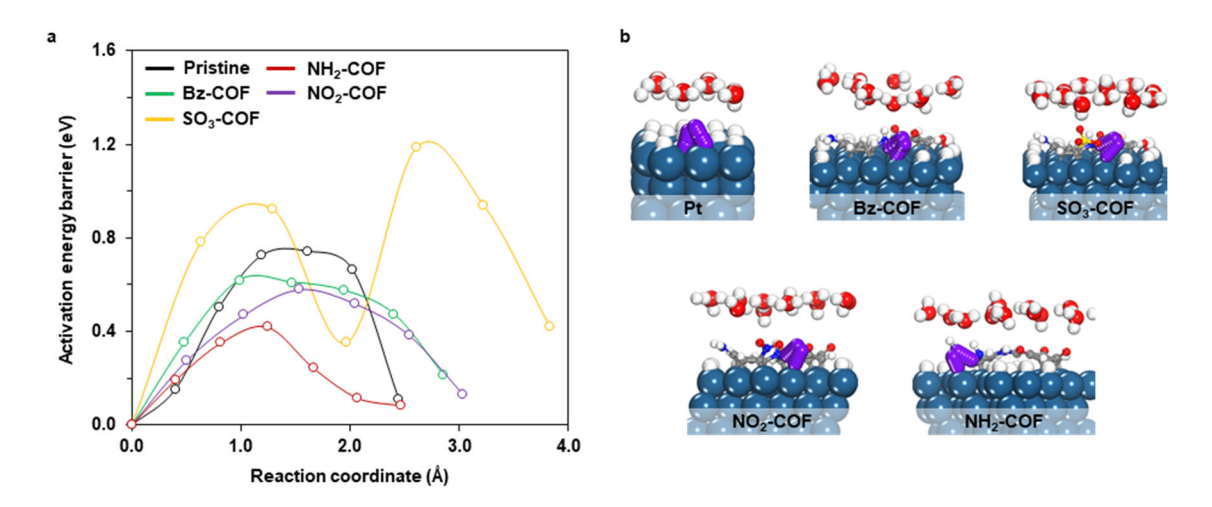


Fig. S27. (a) Calculated activation energy of the Tafel step and (b) proton configurations on Pt surfaces with and with COFs in the presence of hydronium ion (H₃O⁺).

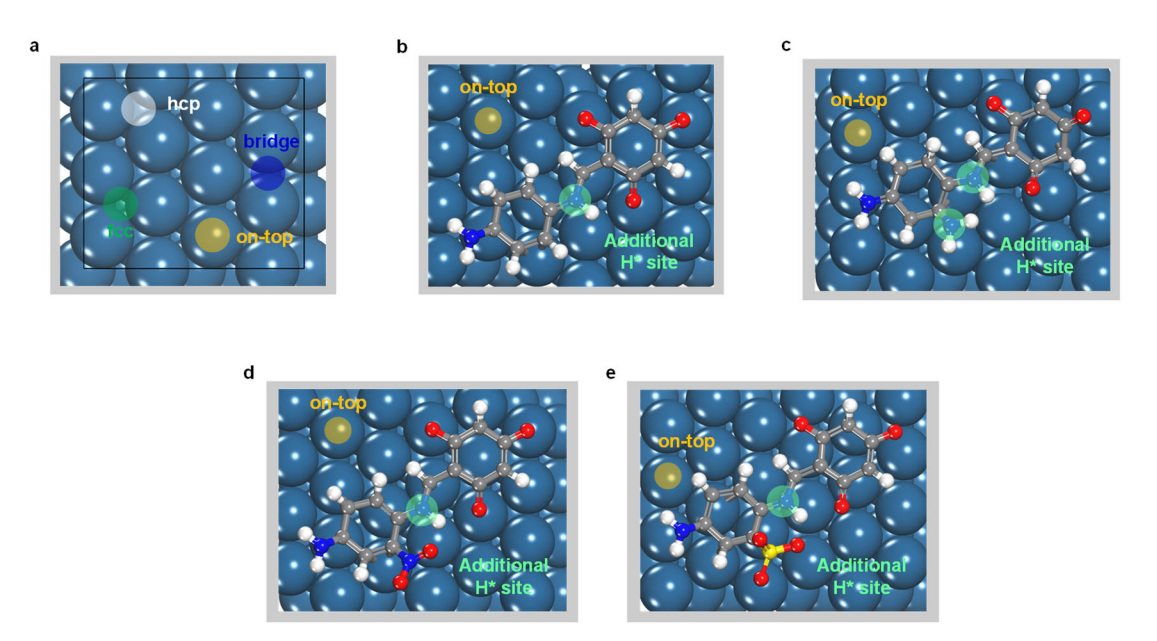


Fig. S28. Possible HER active sites of Pt modified by the COFs: (a) no COF, (b) Bz-COF, (c) NH₂-COF, (d) NO₂-COF, and (e) SO₃-COF.

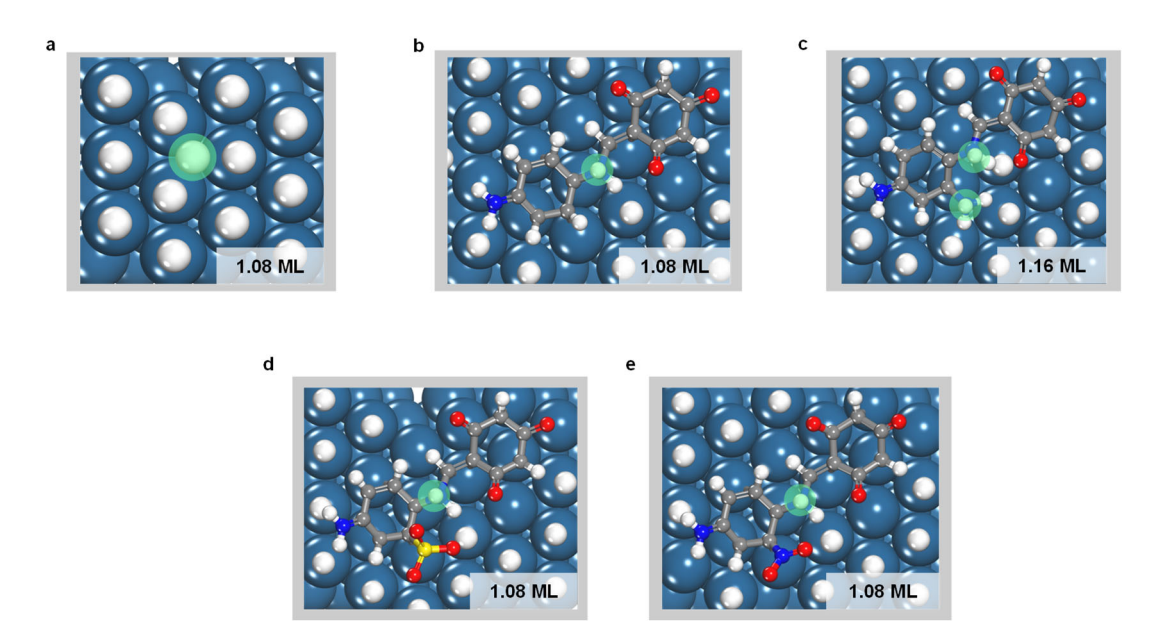


Fig. S29. Optimized H* binding site of Pt modified by different COFs: (a) no COF, (b) Bz-COF, (c) NH₂-COF, (d) SO₃-COF, and (e) NO₂-COF. Green circles indicate the optimized sites.

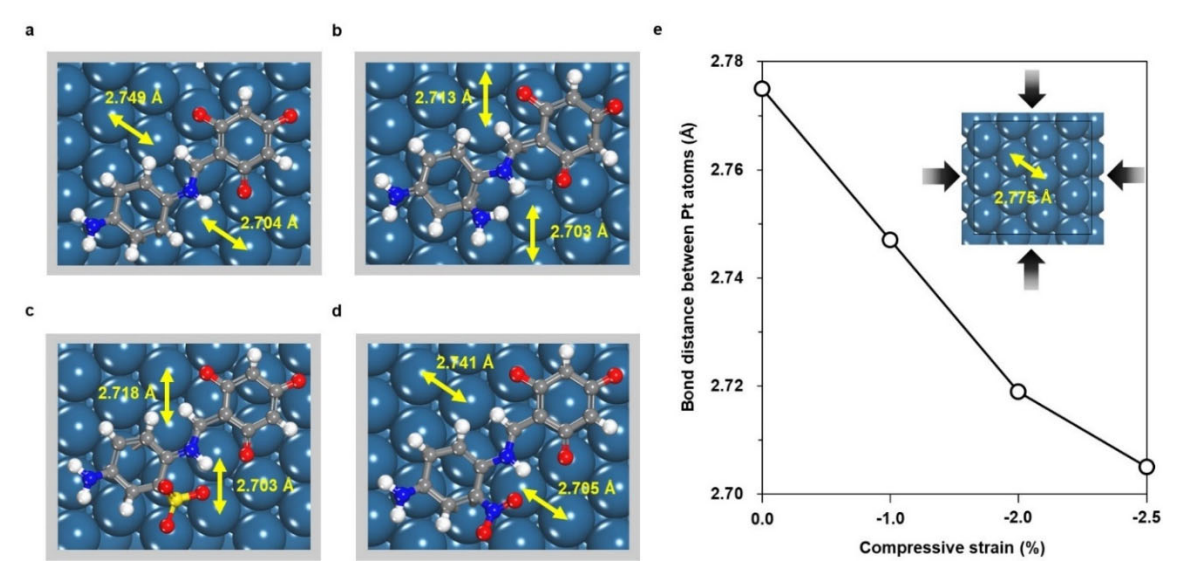


Fig. S30. Pt-Pt distances of Pt surface modified by (a) Bz-COF, (b) NH₂-COF, (c) SO₃-COF, and (d) NO₂-COF, respectively. (e) Plot of Pt-Pt distance as a function of compressive strain (Inset: pristine Pt surface and the corresponding Pt-Pt distance).

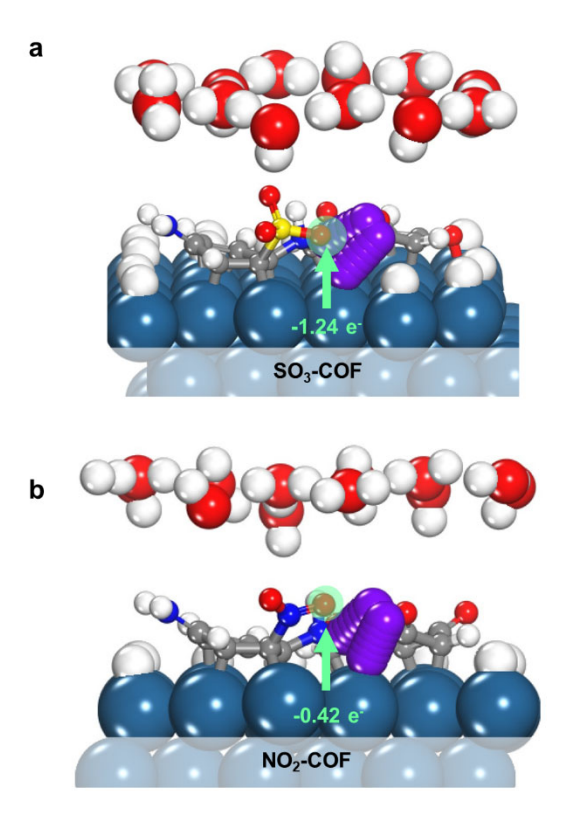


Fig. S31. Illustrations of interactions between oxygen and proton in the formation of molecular hydrogen catalyzed Pt modified with (a) SO₃-COF and (b) NO₂-COF. Light green circles indicate the accumulated electron charge.

Tables

Table S1. Chemical structure, number of atoms, and molecular weight of the repeating unit of the functionalized COFs used in this study.

Para	meter	Bz-COF	NO ₂ -	NH ₂ - COF	SO ₃ -
Number of atoms/unit	С	36	36	36	36
	Н	24	21	27	24
	N	6	9	9	6
	О	6	12	6	15
	S	-	-	-	3
Molecular weight/unit (g/mol)		636	771	681	876

Table S2. Elemental analysis, H/N and C/N mass ratios of NO₂-COF and NH₂-COF

	NO ₂ -C		NH ₂ -COF (wt%)		
	Experimental	Theoretical	Experimental	Theoretical	
С	52.89	54.9	51.35	54.5	
Н	3.07	2.1	3.42	2.8	
N	15.06	14.8	14.67	14.7	
H/N	0.20	0.14	0.23	0.19	
C/N	3.51	3.7	3.5	3.7	

SI Reference

- (1) E. Skúlason, T. Bligaard, S. Gudmundsdóttir, F. Studt, J. Rossmeisl, F. Abild-Pedersen, T. Vegge, H. Jónsson, J. K. Nørskov, A theoretical evaluation of possible transition metal electro-catalysts for N₂ reduction. Phys. Chem. Chem. Phys. 14 (2012) 1235-1245, https://doi.org/10.1039/C1CP22271F.
- (2) J. Hussain, H. Jónsson, E. Skúlason, Faraday efficiency and mechanism of electrochemical surface reactions: CO₂ reduction and H₂ formation on Pt(111). Faraday Discuss. 195 (2016) 619-636, https://doi.org/10.1039/C6FD00114A.